binding of S protein to ACE2 induces conformational changes of the S, which is inevitable to be correctly processed for fusion activity by proteases. In other words, proteases can successfully induce the fusion activity of S protein only after S-ACE2 binding. Alternatively, protease treatment of virions digests out the S1 portion important for ACE2 binding, resulting in a loss of infectivity, whereas S2 alone is sufficient for fusion after binding to its receptor despite loss of the S1 fragment.

Why is the infection via the endosomal pathway not as efficient as direct infection from the cell surface? Throughout our examinations, replication deriving from the cell surface pathway began 1 h ahead of that via the endosomal pathway. We assume that a virus needs ≈1 h for trafficking from the cell surface where virion binds to ACE2 to the endosome. When cells are infected with an extremely low moi, a condition that occurs in natural infection, a 100- to 1,000-fold higher rate of infection was observed in the presence of proteases. Thus a 10-fold difference at 6 h after inoculation could result in a 1,000-fold difference, provided that one cycle of SARS-CoV replication is ≈6 h (25) and three rounds of infection take place within 20 h.

The present studies suggest that coinfection of SARS-CoV with some other non- or low-pathogenic respiratory agents, such as *Chlamydia*, mycoplasma, or bacteria, results in severe lung disease, which is attributed to the proteases produced by the infection with those non-SARS-CoV agents, as has been shown by the enhancement of respiratory diseases caused by influenza virus coinfected with nonpathogenic bacteria (26, 27). Studies are in progress to see whether coinfection exacerbates pneumonia in mice infected with SARS-CoV.

We thank Miyuki Kawase for excellent technical assistance throughout the experiments, John Ziebuhr (University of Würzburg, Würzburg, Germany) for providing SARS-CoV Frankfurt-1, and Judith White (University of Virginia, Charlottesville) for valuable comments on this work. We also thank the colleagues of our institute, especially Shuetsu Fukushi, Keiko Nakagaki, Kohji Ishii, and Yasuko Yokota, for valuable discussions and encouragement throughout the research. This work was supported by Ministry of Education, Culture, Sports, Science, and Technology Grant 16017308 and Ministry of Health, Labor, and Welfare Grant H16-Shinkoh-9.

1. Ksiazek, T .G., Erdman, D., Goldsmith, C., Zaki, S. R., Peret, T., Emery, S., Tong, S., Urbani, C., Comer, J. A., Lim, W., *et al.* (2003) *N. Engl. J. Med.* **348,** 1953–1966.
2. Drosten, C., Gunther, S., Preiser, W., Van Der Werf, S., Brodt, H. R., Becker, S., Rabenau, H., Panning, M., Kolesnikowa, L., Fouchier, R. A., *et al.* (2003) *N. Engl. J. Med.* **348,** 1967–1976.
3. Marra, M. A., Jones, S. J., Astell, C. R., Holt, R. A., Brooks-Wilson, A., Buttefield, Y. S., Khattra, J., Asano, J. K., Barber, S. A., Chan, S. Y., *et al.* (2003) *Science* **300,** 1399–1404.
4. Rota, P. A., Oberste, M. S., Monroe, S. S., Nix, W. A., Campagnoli, R., Icenogle, J. P., Penaranda, S., Bankamp, B., Maher, K., Chen, M. H., *et al.* (2003) *Science* **300,** 1394–1399.
5. The Chinese SARS Molecular Epidemiology Consortium (2004) *Science* **303,** 1666–1669.
6. Peiris, J. S., Guan, Y. & Yuen, K. Y. (2005) *Nat. Med.* **10,** 588–597.
7. Lai, M. M. C. & Cavanagh, D. (1997) *Adv. Virus Res.* **48,** 1–100.
8. Tyrell, D. A. J., Almeida, J. D., Berry, D. M., Cunningham, C. H., Hamre, D., Hofstad, M. S., Mallucci, L. & McIntosh, K. (1968) *Nature* **220,** 650.
9. Gallagher, T. M., Escarmis, C. & Buchmeier, M. J. (1991) *J. Virol.* **65,** 1916–1928.
10. Simmons, G., Reeves, J. D., Rennekamp, A. J., Amberg, S. M., Piefer, A. J. & Bates, P. (2004) *Proc. Natl. Acad. Sci. USA* **101,** 4240–4245.
11. Matsuyama, S. & Taguchi, F. (2000) *Virology* **273,** 80–89.
12. Kawabata, K., Haio, T. & Matsuoka, S. (2002) *Eur. J. Pharmacol.* **451,** 1–10.
13. Wong, C. K., Lam, C. W., Wu, A. K., Ip, W. K., Lee, N. L., Chan, I. H., Lit, L. C., Hui, D. S., Cha, M. H., Chung, S. S., *et al.* (2004) *Clin. Exp. Immunol.* **136,** 95–103.
14. Nicholls, J. M., Poon, L. L., Lee, K. C., Ng, W. F., Lai, S. T., Leung, C. Y., Chu, C. M., Hui, P. K., Mak, K. L., Lim, W., *et al.* (2003) *Lancet* **361,** 1773–1778.
15. Peiris, J. S. M., Lai, S. T., Poon, L. L. M., Guan, Y., Yam, L. Y. C., Lim, W., Nicholls, J., Yee, W. K. S., Yan, W. W., Cheung, M. T., *et al.* (2003) *Lancet* **361,** 1767–1772.
16. Tse, G. M., To, K. F., Chan, P. K., Lo, A. W., Ng, K. C., Wu, A., Lee, N., Wong, H. K., Mac, S. M., Chan, K. F., *et al.* (2004) *J. Clin. Pathol.* **57,** 260–265.
17. To, K. F. & Lo, A. W. (2004) *J. Pathol.* **203,** 740–743.
18. Li, W., Moore, M. H., Vasilieva, N., Sui, J., Wong, S. K., Berne, M. A., Somasundaran, M., Sullivan, J. L., Luzuriaga, K., Greenough, T. C., *et al.* (2003) *Nature* **426,** 450–454.
19. Zhan, J., Chen, W., Li, C., Wu, W., Li J., Jiang, S., Wang, J., Zeng, Z., Huang, Z. & Huang, H. (2003) *Clin. Med. J.* **116,** 1265–1266.
20. Leung, W. K., To, K. F., Chan, P. K., Chan, H. L., Wu, A. K., Lee, N., Yuen, K. Y. & Sung, J. J. (2003) *Gastroenterology* **125,** 1011–1017.
21. Rott, R., Orlich, M. & Blodorn, J. (1975) *Virology* **68,** 426–439.
22. Nagai, Y., Klenk, H. D. & Rott, R. (1976) *Virology* **72,** 494–508.
23. Ohuchi, M. & Homma, M. (1976) *J. Virol.* **18,** 1147–1150.
24. Tashiro, M., Yokogoshi, Y., Tomita, K., Seto, J. T., Rott, R. & Hido, H. (1992) *J. Virol.* **72,** 11–16.
25. Ng, M.-L., Tan, S.-H., See, E. E., Ooi, E. E. & Ling, A. E. (2003) *J. Gen. Virol.* **84,** 3291–3303.
26. Tashiro, M., Ciborowski, P., Klenk, H.-D., Pulverer, G. & Rott, R. (1987) *Nature (London)* **325,** 536–537.
27. Kishida, N., Sakoda, Y., Eto, M., Sunaga, Y. & Kida, H. (2004) *Arch. Virol.* **149,** 2095–2140.

JOURNAL OF VIROLOGY, May 2005, p. 6102–6110 Vol. 79, No. 10
0022-538X/05/$08.00+0 doi:10.1128/JVI.79.10.6102–6110.2005

Receptor-Independent Spread of a Highly Neurotropic Murine Coronavirus JHMV Strain from Initially Infected Microglial Cells in Mixed Neural Cultures

Keiko Nakagaki,[1] Kazuhide Nakagaki,[2] and Fumihiro Taguchi[1]*

National Institute of Infectious Diseases, Murayama Branch, 4-7-1 Gakuen, Musashi-Murayama, Tokyo 208-0011,[1] and Nippon Veterinary and Animal Science University, College of Veterinary Medicine, 1-7-1 Kyonancho, Musashino, Tokyo 180-8602,[2] Japan

Received 12 October 2004/Accepted 3 December 2004

Although neurovirulent mouse hepatitis virus (MHV) strain JHMV multiplies in a variety of brain cells, expression of its receptor carcinoembryonic antigen cell adhesion molecule 1 (CEACAM 1) (MHVR) is restricted only in microglia. The present study was undertaken to clarify the mechanism of an extensive JHMV infection in the brain by using neural cells isolated from mouse brain. In contrast to wild-type (wt) JHMV, a soluble-receptor-resistant mutant (srr7) infects and spreads solely in an MHVR-dependent fashion (F. Taguchi and S. Matsuyama, J. Virol. 76:950–958, 2002). In mixed neural cell cultures, srr7 infected a limited number of cells and infection did not spread, although wt JHMV induced syncytia in most of the cells. srr7-infected cells were positive for GS-lectin, a microglia marker. Fluorescence-activated cell sorter analysis showed that about 80% of the brain cells stained with anti-MHVR antibody (CC1) were also positive for GS-lectin. Pretreatment of those cells with CC1 prevented virus attachment to the cell surface and also blocked virus infection. These results show that microglia express functional MHVR that mediates JHMV infection. As expected, in microglial cell-enriched cultures, both srr7and wt JHMV produced syncytia in a majority of cells. Treatment with CC1 of mixed neural cell cultures and microglia cultures previously infected with wt virus failed to block the spread of infection, indicating that wt infection spreads in an MHVR-independent fashion. Thus, the present study indicates that microglial cells are the major population of the initial target for MHV infection and that the wt spreads from initially infected microglia to a variety of cells in an MHVR-independent fashion.

An initial event in viral infection is the binding of virus to target cells, which is mediated by the binding of a virion surface protein with its specific receptor on the cell membrane. Some molecules classified in the immunoglobulin superfamily are functional receptors for various viruses. CD4 has been identified as a receptor for human immunodeficiency virus (2). In addition, measles virus receptor SLAM (CD150) (34) and carcinoembryonic antigen adhesion molecule 1 (CEACAM1) (mouse hepatitis virus receptor [MHVR]) (4, 36), which serves as a receptor of the murine coronavirus mouse hepatitis virus (MHV), belong to the immunoglobulin superfamily. Although a receptor is an essential molecule in order for a virus to infect, it is not the ultimate determinant for susceptibility of the cell.

MHV, a member of the coronavirus family, is an enveloped virus with single-stranded, positive-sense genomic RNA that is about 30 kilobases long (13). Spike (S) protein, composed of virion projections, is responsible for binding to a receptor and also for the cell entry mechanism of MHV. S protein is a type I glycoprotein of 180 to 200 kDa in molecular mass that is cleaved by host cell-derived protease into two subunits, N-terminal S1 and C-terminal S2 (27). The N-terminal region of the S1, called S1N330, is involved in receptor binding (12, 29), which triggers fusogenic activation accompanied by conformational changes of the membrane-anchored S2 subunit (15). The cell entry mechanism of MHV is thought to be similar to that of human immunodeficiency virus or other enveloped viruses (24).

Four different splice variants of MHVR are known to exist. They have either two or four ectodomains with long or short cytoplasmic tails (1, 4). Two allelic forms have been reported; one is CEACAM1a, which is expressed in most laboratory mouse strains, and the other is CEACAM1b, which is known thus far to be expressed by only the SJL mouse strain (3, 39) but is widely expressed in wild mice (19). A region in the N-terminal domain is responsible for virus binding, which is also involved in the homotypic interaction of this molecule (5, 17, 35).

MHV causes different types of diseases, such as hepatitis, enteritis, and encephalomyelitis. Infection in most tissues is thought to be mediated by MHVR, since the distribution of viral protein in the tissue is closely consistent with the MHVR distribution (9). In contrast, some cells expressing MHVR, e.g., epithelial cells in the kidney or respiratory tracts, have not been reported to be the target of MHV infection (9). Severe encephalomyelitis as a result of extensive infection in various brain cells, such as astrocytes, microglia, ependymal cells, neurons, and oligodendrocytes (14, 20, 21, 28), is observed in infection with wild-type (wt) strain JHMV, although only microglial cells were found to express MHVR (22). The srr7 mutant, derived from wt virus, is benign in terms of neurovirulence (16) compared with wt JHMV, and its infection in the brain is restricted. An outstanding difference in the mode of

* Corresponding author. Mailing address: Lab. of Respiratory Viral Diseases and SARS, Department of Virology III, National Institute of Infectious Diseases, Murayama Branch, 4-7-1 Gakuen, Musashi-Murayama, Tokyo 208-0011 Japan. Phone: 81-42-561-0771, ext. 533. Fax: 81-42-567-5631. E-mail: ftaguchi@nih.go.jp.

virus spread between wt JHMV and srr7 is that the former spreads in both MHVR-dependent and -independent fashions, whereas srr7 lacks the ability to spread in an MHVR-independent fashion; namely, wt JHMV infection spreads from DBT cells infected via MHVR to MHVR-deficient BHK cells, although srr7 fails to do so (30). The difference in virulence could be due to whether the virus spreads in an MHVR-independent fashion or not, as postulated by Gallagher and Buchmeier (6).

To determine whether the above hypothesis is correct, we have examined in the present study infections with wt virus as well as srr7 in mixed neural cell cultures, which consisted of neurons, astrocytes, microglial cells, and oligodendrocytes. We have confirmed MHVR expression on microglial cells and found that MHVR was a functional receptor. Furthermore, it was revealed that wt virus spreads in neural cell cultures in an MHVR-independent fashion.

MATERIALS AND METHODS

Viruses. A highly neurotropic MHV strain, MHV-JHM cl-2 (designated wt JHMV) (32), and a mutant derived from wt JHMV that is resistant to neutralization by soluble form of MHVR, srr7, were used. srr7 has a single amino acid mutation at position 1114 (Leu to Phe) of the S2 subunit of the S protein relative to wt JHMV (23). These viruses were propagated and titrated using DBT cells maintained in Dulbecco's modified Eagle's minimal essential medium (DMEM) (Gibco, Grand Island, NY) supplemented with 5% fetal bovine serum (FBS) as described previously (33).

Cell separation from mouse cerebrum. Specific-pathogen-free ICR mice were purchased from Charles River (Tokyo, Japan). Primary mixed neural cell culture were established from the forebrains of 1- to 3-day-old neonate mice as described previously, with minor modifications (10). Briefly, newborn mice were decapitated, and their cerebral hemispheres were aseptically collected in DMEM. The hemispheres were minced and incubated for 1 h with dispase (Roche, Branchburg, NJ) and collagenase (Invitrogen Corp., Carlsbad, CA) at 37°C with periodic agitation. After centrifugation, the digested tissue was gently triturated with a pipette and washed twice with Hanks' balanced salt solution (HBSS) (Invitrogen Corp.). Myelin, red blood cells, and cell debris were removed from neural cells by using a Percoll (Pharmacia, Uppsala, Sweden) density gradient. After two washings with HBSS, the cells were used for culture or flow cytometry analysis.

Preparation of cultures enriched with microglial cells or astrocytes. For culture of purified microglia, collected cerebral hemispheres were minced, dissociated with trypsin (Invitrogen Corp.), and then maintained with DMEM supplemented with 10% FBS. After 10 days of culture, microglia were detached from an astrocyte monolayer by gently shaking the culture flask. The floating cells were reseeded in a 16-well chamber slide (Nunc, Naperville, IL) in the same medium. For the preparation of astrocyte-enriched cultures, primary neural cell cultures prepared as described above were vigorously shaken to eliminate microglia, oligodendrocytes, and neural progenitor cells growing over the astrocyte monolayer. After shaking, the supernatant was removed and adherent cells were trypsinized and cultured as astrocyte-rich cells.

Effects of CC1 on initial infection of JHMV strains and on subsequent spread of viruses. Cells (1×10^5) isolated as described above were seeded into a well on a polyethyleneimine-coated, 16-well chamber slide and cultured in DMEM supplemented with B27 (Invitrogen Corp.) for 2 days. Neural cells were incubated in 30 μl of DMEM containing serially 10-fold-diluted anti-MHVR monoclonal antibody (MAb) CC1, kindly provided by Kay Holmes (37), at 37°C for 1 h. The same immunoglobulin G1 (IgG1) isotype directed against an irrelevant protein was used as a control. After removal of the culture medium, cells were inoculated with wt JHMV or srr7 at a multiplicity of infection (MOI) of 5 and incubated in the presence of CC1 for 12 h and 24 h after wt JHMV and srr7 infection, respectively. Cells were then fixed with 4% paraformaldehyde, and viral antigens in cells were visualized by immunohistochemistry using anti-MHV MAb (11) and anti-mouse IgG labeled with horseradish peroxidase. Antigen-positive cells were counted under microscopy. The blockade of viral infection by CC1 was calculated as the percentage of viral antigen-positive cells in the presence of each dilution of CC1, compared with cell numbers obtained in the absence of CC1.

To examine whether CC1 inhibits virus spread from initially infected cells, mixed neural cell cultures, as well as microglial cell-enriched cultures, prepared as described above, were infected with either wt virus or srr7 at an MOI of 0.5 and incubated at 37°C for 1 h. Cells were then washed with HBSS and cultured in the presence or absence of CC1 (1 μg/ml) for 24 h. Viral antigens in cells were observed as described above.

Immunocytochemistry. Primary antibodies used to identify each cell type were as follows: anti-glial fibrillary acidic protein (DAKO Chemical, Denmark) polyclonal antibody for astrocytes, O4 MAb (Chemicon, CA) for oligodendrocytes, and MAP-2 (Chemicon Int. Inc., Temecula, CA) for neurons. Binding of the *Griffonia simplicifolia* lectin (GS-lectin) (Vector Laboratories) was used for microglial cell identification. To detect MHV-specific antigen in cells, mouse anti-MHV MAbs were used. Cells grown on a polyethyleneimine-coated Lab-Tek 16-chamber slide were fixed in 4% paraformaldehyde for 10 min and permeabilized by exposure to 1% Triton X-100 for 60 min. Endogenous peroxidase was quenched with 0.3% hydrogen peroxide in phosphate-buffered saline, pH. 7.2. Before staining with mouse MAb, nonspecific binding was blocked using Mouse on Mouse (Vector Laboratories), and antibody binding was detected with avidin-biotin complex (Vector Laboratories), using amino-ethyl-carbazol (Vector Laboratories) as the chromogen. Finally, cells were counterstained with hematoxylin prior to mounting. In order to identify the MHV-infected cells, immunofluorescence dual staining with viral antigen and a cell-specific marker was employed.

Flow cytometry. Flow cytometry (fluorescence-activated cell sorting [FACS]) was employed for detecting the expression of CEACAM1 and viral attachment to the cell surface and the blockade of the viral attachment by MAb CC1. Nonspecific binding on cerebral cells separated as described above was minimized by blocking with purified rat anti-mouse FcIII/IIR MAb (2.4G2; BD PharMingen, San Diego, CA) and PBS containing 1% FBS for 10 min prior to staining. To detect the viral receptor CEACAM1on the cell surface, cells were incubated in CC1 for 30 min at 4°C, or designated IgG1 isotype-matched controls (BD PharMingen), followed by biotinylated anti-mouse IgG1 and avidin-conjugated phycoerythrin (PE). To detect cell-bound wt JHMV or srr7, the cells were infected at an MOI of 5 and incubated for 1 h at 4°C. Cell-bound viruses were detected with anti-MHV MAb and anti-mouse IgG labeled with Alexafluor 488 (Molecular Probes, Inc., Eugene, OR). Virus-attached cells were dual stained with Alexafluor 488-labeled MAb and an antibody for a cell surface maker. To evaluate the competition by CC1 and virus for the receptor, the cells were pretreated with CC1 for 30 min at 4°C. After three washes, they were incubated with wt JHMV or srr7 for 1 h at 4°C, and this was followed by the addition of a mixture of biotinylated anti-mouse IgG1 and Alexafluor 488-labeled MAb against MHV. In addition, after three washes, avidin-PE was added. All stained cells were detected on a FACScan (Becton, Dickinson and Co., NJ) and analyzed with CellQuest software.

Confocal microscopy. Single-plane confocal microscope images were collected using a microscope with an attached krypton/argon mixed-laser unit (Yokogawa Electric Corp.). The gas laser produced excitation wavelengths of 488 nm and 568 nm for Alexafluor 488 and Texas Red, respectively. Individual fluorophore images were merged and pseudocolored using Adobe Photoshop (version 5.5).

RESULTS

Infection of wt JHMV or srr7 in cultured neural cells and blockade of viral infection by MAb CC1. We prepared mixed neural cell cultures from neonatal mouse brain and cultured them for 2 days before virus challenge. To reveal the cell population, we stained the cultivated cells with cell type-specific antibodies or reagents as described in Materials and Methods. Staining revealed that about 40% of the population consisted of neurons; 20%, astrocytes; 20%, microglia; and 1 to 2%, oligodendrocytes. Neuronal progenitor cells were roughly 25% of the total under these culture conditions. We infected the cultivated cells with wt JHMV or srr7, and viral antigens expressed in these cells were monitored by immunocytochemistry using MHV-specific MAbs. As shown in Fig. 1A, viral protein was sporadically detected at 8 h after infection with wt JHMV. The infected cells eventually formed syncytial clusters composed of several cells. The infection rapidly spread with intercellular fusion formation regardless of cell type, and a number of syncytia were observed at 12 h. Twenty-four hours

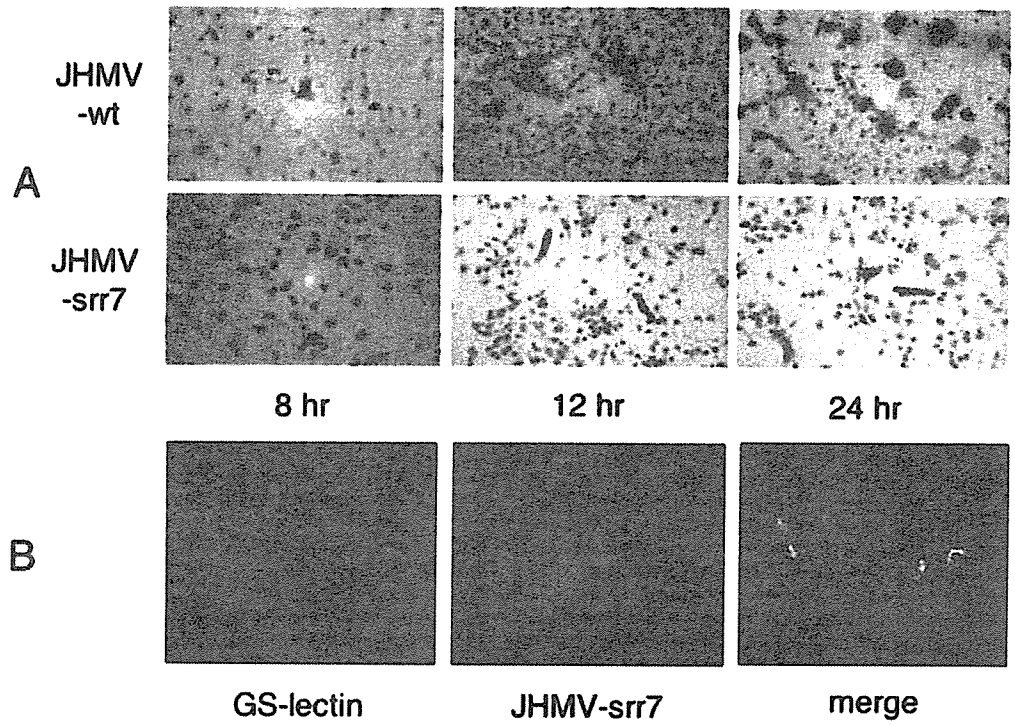

FIG. 1. (A) Infection of mixed neural cell cultures with either wt JHMV or srr7. Mixed neural cell cultures were infected with either wt JHMV or srr7 and fixed with 4% paraformaldehyde at 8 h, 12 h, or 24 h after infection. Viral antigens in cells were detected by staining with anti-MHV MAbs and anti-mouse IgG. (B) Immunofluorescent double staining of srr7-infected cells with anti-MHV MAbs and microglial cell/macrophage-specific GS-lectin. Mixed neural cell cultures were infected with srr7 and incubated at 37°C for 12 h. Viral antigens, as well as microglial cells, were stained with anti-MHV MAbs (Alexafluor 488, green) and GS-lectin (Texas Red, red), respectively, and the images were merged.

after infection, the majority of cells were infected and large syncytia were formed. Unlike those in wt JHMV-infected cells, the viral proteins in srr7-infected cells were not detected as early as 8 h postinoculation. At 12 h viral antigens were observed in only a small proportion of club-like cells, which were morphologically similar to microglial cells. However, srr7 did not induce any intercellular fusion even 24 h after infection. To address whether the cells infected with srr7 observed at 12 h after infection are microglial cells or not, we doubly stained those cell cultures with anti-MHV MAb and GS-lectin, a microglial cell/macrophage marker. Cells with MHV antigen were also stained with GS-lectin (Fig. 1B), which suggested that microglial cells are initially infected by srr7.

We further examined whether the infections caused by these viruses were mediated by MHVR. At first, cell cultures were pretreated with serially diluted anti-MHVR MAb CC1 and challenged with wt JHMV and srr7. Infections in these cells were then monitored by the presence of viral antigens. As shown in Fig. 2, infection with either virus was blocked by pretreatment of CC1 in a concentration-dependent fashion. CC1 at a concentration of 1 to 10 μg/ml (dilution of 10^3 to 10^2) almost entirely prevented infection by either wt JHMV or srr7. It was thus concluded from these observations that the initial infections with wt or srr7 JHMV in neural cells are mediated by MHVR, making the process similar to that with MHV infection in hepatocytes or lymphoid tissue (9).

Identification of cell types expressing MHVR and those to which the viruses attach. The data above indicated that wt JHMV infected various neural cells, while srr7 infected at least microglial cells. Since the wt infection could result from

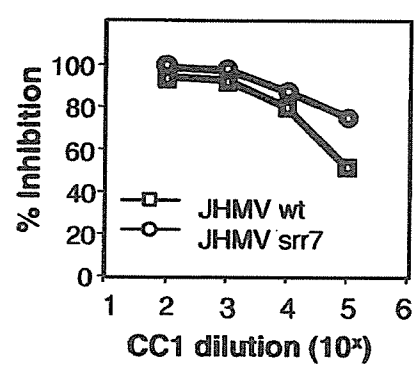

FIG. 2. Blockade of wt and srr7 infection in mixed neural cell cultures by anti-MHVR MAb CC1. Mixed neural cell cultures were treated with 10-fold-stepwise-diluted CC1 at 37°C for 1 h and then infected with either wt virus or srr7. After infection, cells were cultured in the presence of CC1. Viral antigen was visualized by staining with anti-MHV MAbs at 12 and 24 h after wt and srr7 infection, respectively, and antigen-positive cells were counted. The blockade of viral infection by CC1 was calculated as the percentage of viral antigen-positive cells in the presence of CC1 compared with cell numbers obtained in the absence of CC1

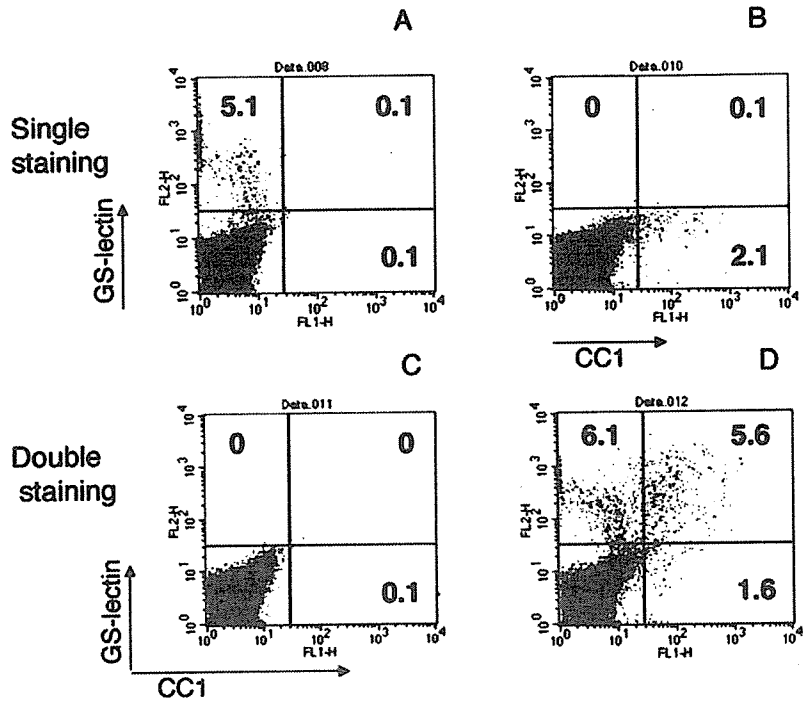

FIG. 3. Examination of MHVR-bearing cells by flow cytometric analysis. Neural cells separated from cerebrums of 1- to 3-day-old mice were labeled with either GS-lectin (PE) (A) or anti-MHVR MAb CC1 (Alexafluor 488) (B). Cells were also analyzed for coexpression of GS-lectin and MHVR (D) by double staining as described in Materials and Methods. (C) Background control.

MHVR-independent infection, we have focused on the microglial cells that were infected by srr7. Thus, microglial cells were first evaluated by FACS as MHVR-bearing cells. Cells isolated from the cerebrums of neonatal mice were directly examined for the presence of MHVR by using CC1. Simultaneously, those cells were also examined by using GS-lectin binding. MHVR-expressed and GS-lectin-binding cells were revealed to consist of 2.1% and 5.1% of the total cells, respectively (Fig. 3). Double staining with CC1 and GS-lectin revealed that approximately 78% of the MHVR-bearing cells were GS-lectin-positive microglial cells. These results also demonstrated that half of the microglial cells are MHVR positive, indicating that the major population expressing MHVR consists of microglial cells.

We further examined, using FACS, the cell types that permit attachment of JHMV as well as those that express GS-lectin. Neural cells prepared as described above were mixed with wt JHMV, and cells bound by viruses were monitored by anti-spike MAbs. It was demonstrated that the percentages of cells allowing the attachment of JHMV and those that were GS-lectin positive were 1.2% and 3.8%, respectively (Fig. 4A and B). It was also shown that double-positive cells consisted of 1%, covering more than 83% of the cells bound by virus, suggesting that most of the cells bound with JHMV are microglial cells. We then examined by FACS whether or not pretreatment of these cells with CC1 prevents JHMV attachment on the cell surface. Cells were first treated or not treated with CC1 at 4°C and then infected with wt JHMV. The binding of CC1 and that of JHMV were determined by using antibodies against CC1 and JHMV, respectively. Figure 4C, D, and E show that the percentage of cells allowing JHMV attachment decreased from 1.3% without treatment with CC1 to almost 0% if these cells were pretreated with CC1, indicating that wt JHMV attaches to neural cells via MHVR but not through other molecules on the cell surface.

Taken together, these findings suggest that both wt and srr7 initially infect microglial cells via MHVR expressed on their surface, and there is very little chance that JHMV infection is mediated by molecules other than MHVR. It is also suggested that MHVR expressed on cells other than microglial cells (consisting of 22% of cells expressing CEACAM1) would play a role in the initial infection with JHMV.

Virus infection in cultures enriched with microglial cells. The results described above suggested that MHVR-positive cells, mostly microglial cells, are initial target cells for wt and srr7 in mixed neural cell cultures. It is also postulated that wt JHMV spreads in an MHVR-independent manner but that srr7 fails to do so in mixed neural cell cultures. If this is the case, both of these viruses are thought to spread efficiently in cell cultures enriched with microglial cells, half of which are shown to be MHVR positive. A culture established by shaking the mixed neural cells usually contains more than 95% GS-lectin positive microglial cells. We infected this culture with either wt JHMV or srr7 and monitored viral spread by the appearance of syncytial cells as well as viral antigens in cells. As shown in Fig. 5, cultures prepared as described above consisted predominantly of microglial cells as revealed by GS-lectin-positive binding. In this culture, both wt and srr7 produced similarly large numbers of syncytia, including approximately 50% of the cultured cells, and those cells were also GS-lectin

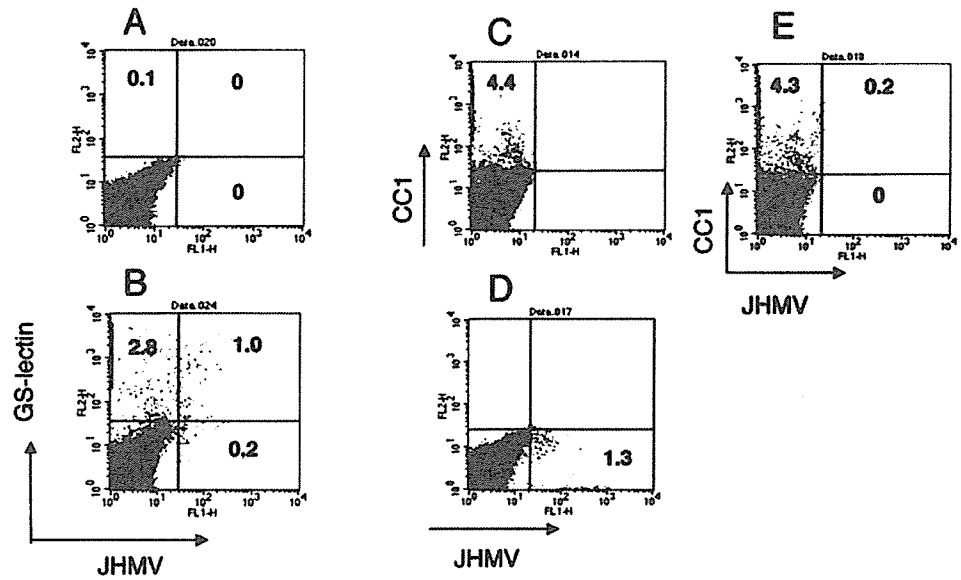

FIG. 4. (A and B) Detection of MHVR and JHMV binding to cells by flow cytometric analysis. Cells isolated from neonate mouse brain were mixed with wt JHMV and stained with anti-MHV MAb–Alexafluor 488. Those cells were also examined for binding by GS-lectin PE and analyzed by flow cytometry (B). (A) Background control. (C to E) Inhibition of wt JHMV attachment on neural cells by CC1. Cells isolated from neonatal mice were first treated with CC1 at 4°C for 30 min and then infected with wt JHMV. JHMV attached to cells was detected with anti-MHV MAb, biotinylated anti-mouse IgG1, and avidin-PE (E). As a control, cells single stained with CC1 (C) or those with attached virions (D) were also analyzed by flow cytometry.

positive. These findings indicated that both viruses spread and induced syncytia efficiently in microglial cultures, in a manner similar to that of infection in MHVR-positive DBT cells.

Virus infection in astrocyte-enriched cultures. Several reports have described that astrocyte-enriched cultures support JHMV infection (21), although microglial cell contamination in this culture was not thoroughly excluded. We infected astrocyte-enriched cultures, prepared as described in Materials and Methods, with wt and srr7. As shown in Fig. 6A, wt infection induced syncytium formation. Although srr7 failed to induce syncytia, viral infection was evidenced by detection of the antigen in a few cells infected with srr7 (Fig. 6A). These ob-

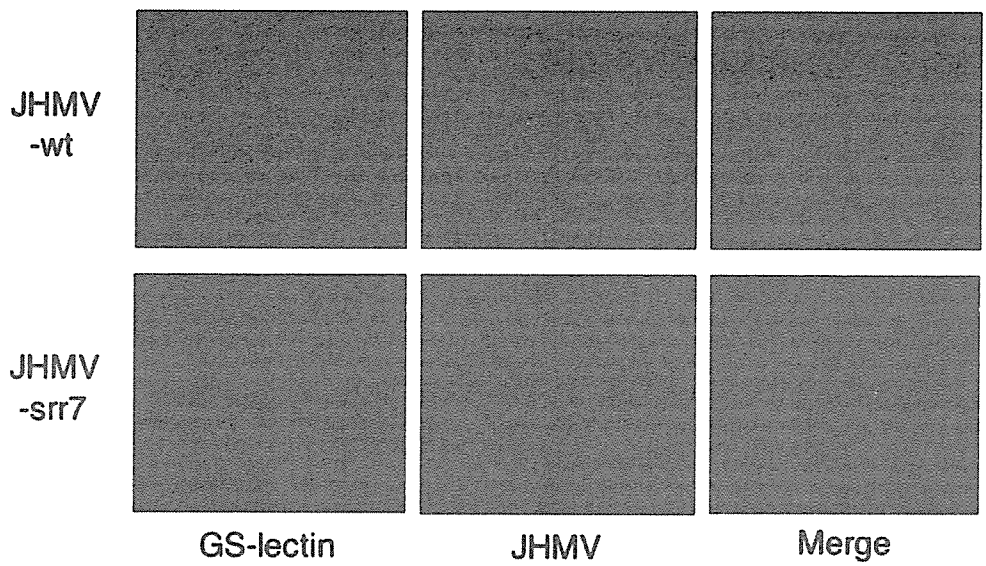

FIG. 5. Infection of microglial cell-enriched cultures by wt JHMV or srr7. Microglial cell-enriched cultures were prepared as described in Materials and Methods. Those cells were infected with either wt JHMV or srr7, and viral antigens were examined with anti-MHV MAb (Texas Red) as well as for the presence of GS-lectin (Alexafluor 488) on the cultured cells at 12 h after infection. The images of GS-lectin-positive and MHV-positive cells were merged.

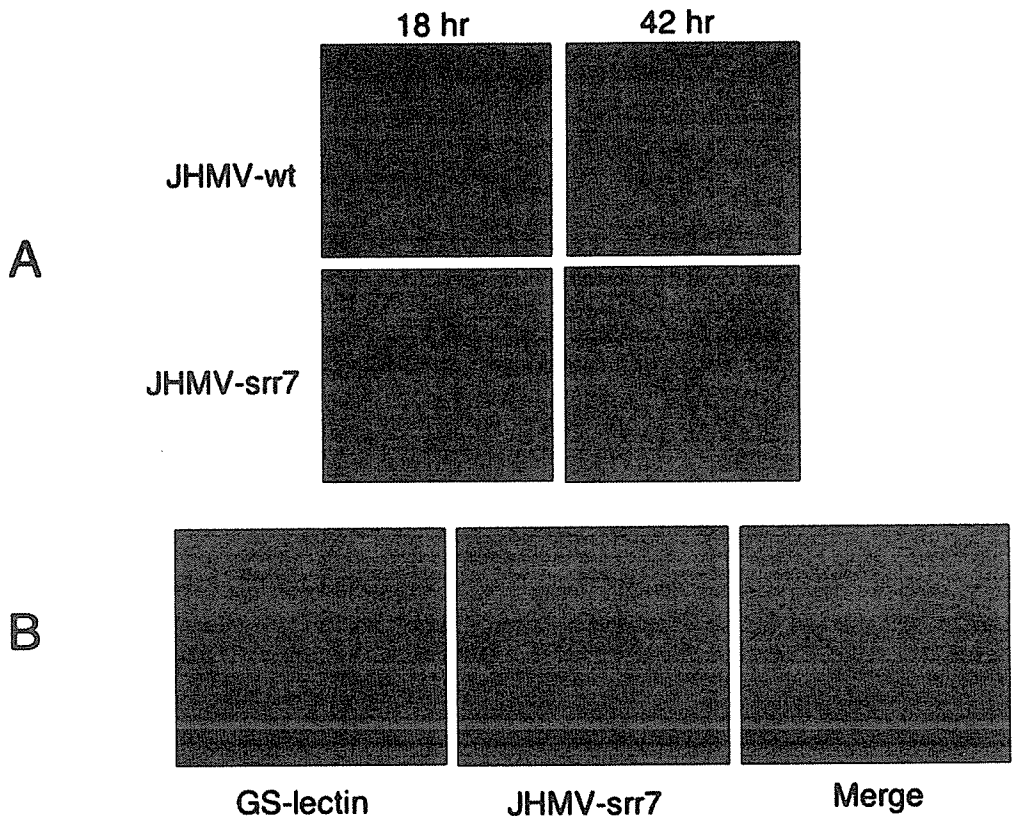

FIG. 6. (A) Infection of astrocyte-enriched cultures by wt and srr7. Astrocyte cultures were prepared as described in Materials and Methods. Cells were infected with either wt JHMV or srr7, and viral antigens were monitored with anti-MHV MAb (Alexafluor 488) at 12 h after infection. (B) Infection of srr7 in astrocyte-rich cultures. srr7-infected cells in astrocyte-rich cultures were also examined for GS-lectin positivity (using Texas Red) as well as with anti-MHV MAb. These two images were merged.

servations were very similar to those recorded for infection in mixed neural cell cultures. We next tried to test whether srr7-infected cells are microglial cells or not. As shown in Fig. 6B, srr7 antigen-positive cells were revealed to be GS-lectin positive, showing that srr7 infected solely microglial cells mingled within the astrocyte culture. This strongly suggests that initial infection in astrocyte culture takes place in microglial cells as well. Wt infection could spread to astrocytes in an MHVR-independent fashion, while srr7 infection was restricted among microglia.

Effects of CC1 treatment on virus spread from initially infected cells. The data presented above suggest that wt virus spreads from initially infected microglial cells to MHVR-negative cells existing in mixed neural cell cultures, while srr7 infection is restricted to MHVR-positive microglial cells. To see whether this is the case or not, we examined whether CC1 could inhibit the spread of wt infection from the initially infected cells. Mixed neural cell cultures infected with wt virus 1 h previously were cultured with medium in the presence or absence of CC1. Cells were then immunochemically stained using anti-MHV MAb to see the spread of virus infection. As shown in Fig. 7A, there was no substantial difference in the proportion of MHV antigen-positive syncytia between cells cultured in the presence and absence of CC1, indicating that wt virus spread from initially infected cells was not prevented by CC1. We also did a similar experiment using either wt- or srr7-infected microglial cell cultures, and about 50% of those expressed MHVR. As shown in Fig. 7B, CC1 prevented the spread of srr7, while it failed to prevent the wt virus spread in a way observed in srr7 infection, although CC1 treatment reduced wt syncytium formation to a certain extent. This reduction could be due to the prevention of an MHVR-dependent infection in microglial cells. These results clearly showed that wt virus spread from initially infected cells to a variety of cells in an MHVR-independent fashion, while srr7 infection was solely MHVR dependent.

DISCUSSION

The neurotropic MHV strain JHMV induces encephalomyelitis by infecting a wide spectrum of brain cells (14, 20, 25, 28), although except for microglia, MHVR has not been reported to exist on these neural cells (22). Extensive replication of highly neurotropic JHMV in various cells in the mouse brain could be due to the existence of another functional MHV receptor different from MHVR. However, in vivo and in vitro experiments have shown that infection of glial progenitors, oligodendrocytes and astrocytes, was blocked by pretreatment with anti-MHVR antibody MAb CC1 or Ab-655 (9), strongly

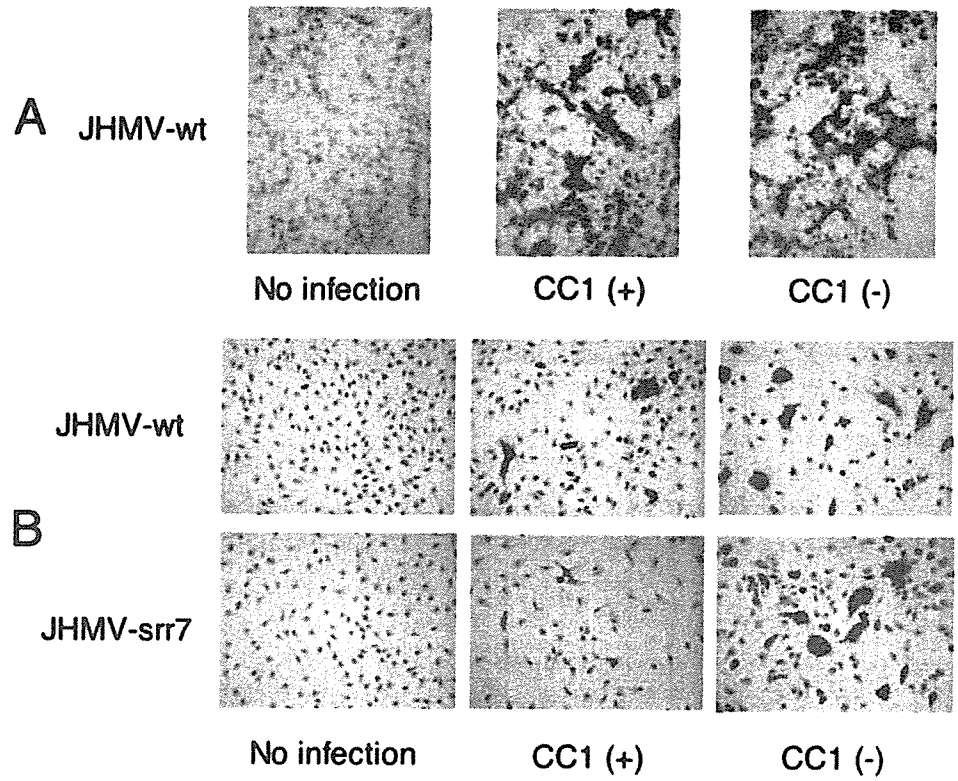

FIG. 7. (A) Effect of CC1 on wt virus spread from initially infected cells. Mixed neural cell cultures were infected with wt virus. After 1 h of adsorption, cells were washed with HBSS and cultured in the presence or absence of CC1. Cells were fixed at 24 h after infection and stained with anti-MHV MAbs. (B) Effect of CC1 on the spread of wt virus and srr7 from initially infected cells in microglial cell-enriched cultures, which were infected with either the wt or srr7 and incubated at 37°C for 1 h. After washing, cells were cultured with medium in the presence or absence of CC1. Cells were stained with anti-MHV MAbs at 24 h after infection.

suggesting that MHVR is essential for the initiation of MHV infection in the brain.

In the present study, we have confirmed the observation of Ramarkrishna et al. (22) that MHVR is expressed on microglial cells, and we have further revealed that MHVR on microglia is a functional receptor. These observations strongly suggest that microglial cells are an initial target of MHV in mixed neural cell cultures and the brain as well. We furthermore showed that wt virus spread from initially infected microglial cells to other types of neural cells without MHVR expression in an MHVR-independent fashion, while srr7 virus lacked this activity. An MHVR-independent infection could contribute to the high neurovirulence of wt virus for mice by infecting a wide spectrum of neural cells in the brain, as was previously suggested by Gallagher and Buchmeier (6).

In double-staining experiments, FACS analysis showed that most, if not all, MHVR-bearing cells were GS-lectin-positive microglial cells. It was further shown that the virus attached to the cells expressing MHVR, since attachment of JHMV on cells was blocked by anti-MHVR antibody CC1. MHVR was also crucial for virus replication, since infection was prevented by pretreatment of cells with CC1. These findings strongly suggest that microglial cells are the major initial targets of JHMV. It should also be noted that 20% of the MHVR-positive cells are GS-lectin negative. These unidentified cells could also serve as initial target cells. This population possibly consists of neurons, astrocytes, oligodendrocytes, neural progenitor cells, ependymal cells, or lectin-negative microglial cells. However, in the mixed cell cultures, srr7 did not infect astrocytes or oligodendrocytes, suggesting that it is unlikely that those cells serve as initial targets of JHMV.

The differences in infection in mixed neural cell cultures observed between the wt and srr7 viruses are in the stage of spread from initially infected cells to MHVR-negative cells, since the initial infection with those viruses takes place in a similar fashion, as blocked by CC1 treatment. If some molecule is involved in the spread, then the wt virus would have access to a variety of cells via such a molecule, but srr7 does not. Although we cannot thoroughly rule out such a possibility, this variation could be explained by their different modes of infection, namely, MHVR-independent infection by wt virus versus MHVR-dependent infection by srr7. The minor effect of CC1 treatment on wt virus spread from initially infected cells to the whole culture clearly indicates the MHVR-independent spread of wt virus, while the inhibitory effect of CC1 on srr7 infection in microglial cell cultures suggests an MHVR-dependent spread of srr7. These differences are similar to those observed in cultured cell lines (7, 18, 30, 31).

Microglia have various markers, depending on their different stages, and they retain functional changes similar to those

seen in other tissue macrophages. Of the various markers, the GS-lectin marker was used in this experiment, because it is expressed on microglial cells throughout all of their stages (26, 38). However, it is also one of the markers for endothelial cells (26), and those cells, in the brain, have been already reported to express MHVR and to be attached by the virus as determined by a direct binding assay on thin sections (8). The cultures prepared in our experiment did not include endothelial cells, as examined by using factor VIII-positive cells (data not shown), a marker of endothelial cells. Thus, the GS-lectin-positive cells used in our study were considered microglial cells.

This study shows that either strain of the virus attached to only 1 to 2% of the whole cells separated from the mouse cerebrum. This number represents less than half of the MHVR-positive cells. Godfraind et al. (9) have reported the existence of MHVR-bearing cells but not susceptible cells such as those of the thyroid gland or epithelial cells of the respiratory tract. It is not evident at present what causes this observed difference between susceptible and unsusceptible MHVR-bearing cells, but it could be possible that some other, as-yet-unidentified, host factor(s) could contribute to the sensitivity to MHV infection.

This study showed that wt virus spreads to various types of cells in culture, and conceivably in the mouse brain, by an MHVR-independent mechanism of infection. Studies are in progress to test whether or not MHVR-independent infection contributes to the high neuropathogenicity of wt JHMV in mice.

ACKNOWLEDGMENTS

We greatly thank Kay Holmes for the MHVR-specific MAb (CC-1).

This work was partly supported by a grant (Urgent Research on the Diagnosis and Test Techniques for SARS) from the Ministry of Education, Science, Sports and Culture of Japan.

REFERENCES

1. **Beauchemin, N., P. Draber, G. Dveksler, P. Gold, S. Gray-Owen, F. Grunert, S. Hammarstrom, K. V. Holmes, A. Karlsson, M. Kuroki, S. H. Lin, L. Lucka, S. M. Najjar, M. Neumaier, B. Obrink, J. E. Shively, K. M. Skubitz, C. P. Stanners, P. Thomas, J. A. Thompson, M. Virji, S. von Kleist, C. Wagener, S. Watt, and W. Zimmermann,** 1999. Redefined nomenclature for members of the carcinoembryonic antigen family. Exp. Cell Res. **252:**243–249.
2. **Dalgleish, A. G., P. C. Beverley, P. R. Clapham, D. H. Crawford, M. F. Greaves, and R. A. Weiss,** 1984. The CD4 (T4) antigen is an essential component of the receptor for the AIDS retrovirus. Nature **312:**763–767.
3. **Dveksler, G. S., C. W. Dieffenbach, C. B. Cardellichio, K. McCuaig, M. N. Pensiero, G. S. Jiang, N. Beauchemin, and K. V. Holmes,** 1993. Several members of the mouse carcinoembryonic antigen-related glycoprotein family are functional receptors for the coronavirus mouse hepatitis virus A59. J. Virol. **67:**1–8.
4. **Dveksler, G. S., M. N. Pensiero, C. B. Cardellichio, R. K. Williams, G. S. Jiang, K. V. Holmes, and C. W. Dieffenbach,** 1991. Cloning of the mouse hepatitis virus (MHV) receptor: expression in human and hamster cell lines confers susceptibility to MHV. J. Virol. **65:**6881–6891.
5. **Dveksler, G. S., M. N. Pensiero, C. W. Dieffenbach, C. B. Cardellichio, A. A. Basile, P. E. Elia, and K. V. Holmes,** 1993. Mouse hepatitis virus strain A59 and blocking antireceptor monoclonal antibody bind to the N-terminal domain of cellular receptor. Proc. Natl. Acad. Sci. USA **90:**1716–1720.
6. **Gallagher, T. M., and M. J. Buchmeier,** 2001. Coronavirus spike proteins in viral entry and pathogenesis. Virology **279:**371–374.
7. **Gallagher, T. M., M. J. Buchmeier, and S. Perlman,** 1992. Cell receptor-independent infection by a neurotropic murine coronavirus. Virology **191:** 517–522.
8. **Godfraind, C., N. Havaux, K. V. Holmes, and J.-P. Coutelier,** 1997. Role of virus receptor-bearing endothelial cells of the blood-brain barrier in preventing the spread of mouse hepatitis virus-A59 into the central nervous system. J. Neurovirol. **3:**428–434.
9. **Godfraind, C., S. G. Langreth, C. B. Cardellichio, R. Knobler, J. P. Coutelier, M. Dubois Dalcq, and K. V. Holmes,** 1995. Tissue and cellular distribution of an adhesion molecule in the carcinoembryonic antigen family that serves as a receptor for mouse hepatitis virus. Lab. Investig. **73:**615–627.
10. **Hirayama, M., D. H. Silberberg, R. P. Lisak, and D. Pleasure,** 1983. Long-term culture of oligodendrocytes isolated from rat corps callosum by percoll density gradient. Lysis by polyclonal antigalactocerebroside serum. J. Neuropathol. Exp. Neurol. **42:**16–28.
11. **Kubo, H., S. Takase-Yoden, and F. Taguchi,** 1993. Neutralization and fusion inhibition activities of monoclonal antibodies specific for the S1 subunit of the spike protein of neurovirulent murine coronavirus JHMV c1-2 variant. J. Gen. Virol. **74:**1421–1425.
12. **Kubo, H., Y. K. Yamada, and F. Taguchi,** 1994. Localization of neutralizing epitopes and the receptor-binding site within the amino-terminal 330 amino acids of the murine coronavirus spike protein. J. Virol. **68:**5403–5410.
13. **Lai, M. M. C., and D. Cavanagh,** 1997. The molecular biology of coronaviruses. Adv. Virus Res. **48:**1–100.
14. **Lavi, E., A. Suzumura, M. Hirayama, M. K. Highkin, D. M. Dambach, D. H. Silberberg, and S. R. Weiss,** 1987. Coronavirus mouse hepatitis virus (MHV)-A59 causes a persistent, productive infection in primary glial cell cultures. Microb. Pathog. **3:**79–86.
15. **Matsuyama, S., and F. Taguchi,** 2002. Receptor-induced conformational changes of murine coronavirus spike protein. J. Virol. **76:**11819–11826.
16. **Matsuyama, S., R. Watanabe, and F. Taguchi,** 2001. Neurovirulence in mice of soluble receptor-resistant (srr) mutants of mouse hepatitis virus: intensive apoptosis caused by less virulent srr mutant. Arch. Virol. **146:**1643–1654.
17. **Miura, H. S., K. Nakagaki, and F. Taguchi,** 2004. N-terminal domain of murine coronavirus receptor CEACAM1is responsible for fusogenic activation and conformational changes of the spike protein. J. Virol. **78:**216–223.
18. **Nash, T. C., and M. J. Buchmeier,** 1996. Spike glycoprotein-mediated fusion in biliary glycoprotein-independent cell-associated spread of mouse hepatitis virus infection. Virology **223:**68–78.
19. **Ohtsuka, N., K. Tsuchiya, E. Honda, and F. Taguchi,** 2001. A study on mouse hepatitis virus receptor genotype in the wild mouse. Adv. Exp. Med. Biol. **494:**237–240.
20. **Parra, B., D. R. Hinton, N. W. Marten, C. C. Bergmann, M. T. Lin, C. S. Yang, and S. A. Stohlman,** 1999. IFN-gamma is required for viral clearance from central nervous system oligodendroglia. J. Immunol. **162:**1641–1647.
21. **Perlman, S., and D. Ries,** 1987. The astrocyte is a target cell in mice persistently infected with mouse hepatitis virus, strain JHM. Microb. Pathog. **3:**309–314.
22. **Ramarkrishna, C., C. C. Bergmann, K. V. Holmes, and S. Stohlman,** 2004. Expression of the mouse hepatitis virus receptor by central nervous system microglia. J. Virol. **78:**7828–7832.
23. **Saeki, K., N. Ohtsuka, and F. Taguchi,** 1997. Identification of spike protein residues of murine coronavirus responsible for receptor-binding activity by use of soluble receptor-resistant mutants. J. Virol. **71:**9024–9031.
24. **Sodroski, J. G,** 1999. HIV-1 entry inhibitors in the side pocket. Cell **99:**243–246.
25. **Stohlman, S. A., C. C. Bergmann, R. C. van der Veen, and D. R. Hinton,** 1995. Mouse hepatitis virus-specific cytotoxic T lymphocytes protect from lethal infection without eliminating virus from the central nervous system. J. Virol. **69:**684–694.
26. **Streit, W. J,** 1990. An improved staining method for rat microglial cells using the lectin Griffonia simplicifonia (GSA I-B4). J. Histochem. Cytochem. **11:** 1683–1686.
27. **Sturman, L. S., C. S. Ricard, and K. V. Holmes,** 1985. Proteolytic cleavage of the E2 glycoprotein of murine coronavirus: activation of cell-fusing activity of virions by trypsin and separation of two different 90K cleavage fragments. J. Virol. **56:**904–911.
28. **Sun, N., and S. Perlman,** 1995. Spread of a neurotropic coronavirus to spinal cord white matter via neurons and astrocytes. J. Virol. **69:**633–641.
29. **Suzuki, H., and F. Taguchi,** 1996. Analysis of the receptor-binding site of murine coronavirus spike protein. J. Virol. **70:**2632–2636.
30. **Taguchi, F., and S. Matsuyama,** 2002. Soluble receptor potentiates receptor-independent infection by murine coronavirus. J. Virol. **76:**950–958.
31. **Taguchi, F., S. Matsuyama, and K. Saeki,** 1999. Difference in Bgp-independent fusion activity among mouse hepatitis viruses. Arch. Virol. **1444:**2041–2049.
32. **Taguchi, F., S. G. Siddell, H. Wege, and V. ter Meulen,** 1985. Characterization of a variant virus selected in rat brains after infection by coronavirus mouse hepatitis virus JHM. J. Virol. **54:**429–435.
33. **Taguchi, F., A. Yamada, and K. Fujiwara,** 1980. Resistance to highly virulent mouse hepatitis virus acquired by mice after low-virulence infection: enhanced antiviral activity of macrophages. Infect. Immun. **29:**42–49.
34. **Tatsuo, H., N. Ono, K., Tanaka, and Y. Yanagi,** 2000. SLAM (CDw150) is a cellular receptor for measles virus. Nature **406:**893–897.
35. **Watt, S. M., A. M. Teixeira, GQ Zhou, R. Doyonnas, Y. Zhang, F. Grunert, R. S. Blumberg, M. Kuroki, K. M. Skubitz, and P. A. Bates,** 2001. Homophilic adhesion of human CEACAM1 inovlves N-terminal domain interactions: structural analysis of the binding site. Blood **98:**1469–1479.
36. **Williams, R. K., G. S. Jiang, and K. V. Holmes,** 1991. Receptor for mouse

hepatitis virus is a member of the carcinoembryonic antigen family of glycoproteins. Proc. Natl. Acad. Sci. USA 88:5533–5536.
37. **Williams, R. K., G. S. Jiang, S. W. Snyder, M. F. Frana, and K. V. Holmes,** 1990. Purification of the 110-kilodalton glycoprotein receptor for mouse hepatitis virus (MHV) A59 from mouse liver and identification of a nonfunctional, homologous protein in MHV-resistant SJL/J mice. J. Virol. **64:** 3817–3823.
38. **Wu, C. H., C. Y. Wen, J. Y. Shieh, and E. A. Ling,** 1992. A quantitative and morphometric study of the transformation of amoeboid microglia into ramified microglia in the developing corpus callosum in rats. J. Anat. **181:**423–430.
39. **Yokomori, K., and M. M. Lai,** 1992. The receptor for mouse hepatitis virus in the resistant mouse strain SJL is functional: implications for the requirement of a second factor for viral infection. J. Virol. 66:6931–6938.

Journal of General Virology (2005), 86, 2269–2274 DOI 10.1099/vir.0.80955-0

Short Communication

Vesicular stomatitis virus pseudotyped with severe acute respiratory syndrome coronavirus spike protein

Shuetsu Fukushi,[1] Tetsuya Mizutani,[1] Masayuki Saijo,[1] Shutoku Matsuyama,[2] Naoko Miyajima,[2] Fumihiro Taguchi,[2] Shigeyuki Itamura,[3] Ichiro Kurane[1] and Shigeru Morikawa[1]

Correspondence
Shuetsu Fukushi
fukushi@nih.go.jp

Special Pathogens Laboratory, Department of Virology I[1], Laboratory of Respiratory Viral Diseases and SARS[2] and Laboratory of Influenza Virus, Department of Virology III[3], National Institute of Infectious Diseases, Gakuen 4-7-1, Musashimurayama, Tokyo 208-0011, Japan

Severe acute respiratory syndrome coronavirus (SARS-CoV) contains a single spike (S) protein, which binds to its receptor, angiotensin-converting enzyme 2 (ACE2), induces membrane fusion and serves as a neutralizing antigen. A SARS-CoV-S protein-bearing vesicular stomatitis virus (VSV) pseudotype using the VSVΔG* system was generated. Partial deletion of the SARS-CoV-S protein cytoplasmic domain allowed efficient incorporation into VSV particles and led to the generation of a pseudotype (VSV-SARS-St19) at high titre. Green fluorescent protein expression was demonstrated as early as 7 h after infection of Vero E6 cells with VSV-SARS-St19. VSV-SARS-St19 was neutralized by anti-SARS-CoV antibody and soluble ACE2, and its infection was blocked by treatment of Vero E6 cells with anti-ACE2 antibody. These results indicated that VSV-SARS-St19 infection is mediated by SARS-CoV-S protein in an ACE2-dependent manner. VSV-SARS-St19 will be useful for analysing the function of SARS-CoV-S protein and for developing rapid methods of detecting neutralizing antibodies specific for SARS-CoV infection.

Received 9 February 2005
Accepted 21 April 2005

Severe acute respiratory syndrome (SARS) is a recently described infectious disease caused by a newly identified coronavirus, SARS-CoV (Drosten *et al.*, 2003; Ksiazek *et al.*, 2003). With a mortality rate of over 9%, SARS has had major health and socio-economic impacts (Fouchier *et al.*, 2003). Despite intensive efforts, no effective antiviral treatments against SARS have yet been established. Studies of SARS-CoV infection have been limited because of the highly infectious nature of the virus and the problem of recent cases in which infection was suspected to have occurred in research laboratories.

Entry of SARS-CoV into susceptible cells is mediated by binding of the viral spike (S) protein to receptor molecules. The SARS-CoV-S protein has a 13 aa signal peptide at its N terminus, a single ectodomain of 1182 aa and a transmembrane region followed by a cytoplasmic domain of 28 aa (Marra *et al.*, 2003; Rota *et al.*, 2003). Recently, pseudotyped retroviruses bearing SARS-CoV-S protein have been generated by several laboratories (Hofmann *et al.*, 2004; Nie *et al.*, 2004; Simmons *et al.*, 2004). It has been shown that these pseudotyped viruses have a cell tropism identical to SARS-CoV and that their infection is dependent on a receptor molecule, angiotensin-converting enzyme 2 (ACE2), indicating that infection is mediated solely by SARS-CoV-S protein. Pseudotyped viruses provide a safe viral entry model because of their inability to produce infectious progeny virus. A quantitative assay of pseudotyped virus infection could facilitate research on SARS-CoV entry, cell tropism and neutralizing antibodies. Interestingly, it was reported that a pseudotyped retrovirus bearing a SARS-CoV-S protein variant with a truncation in the cytoplasmic domain was incorporated more efficiently into retrovirus particles than the full-length S protein (Giroglou *et al.*, 2004; Moore *et al.*, 2004).

Another pseudotyping system with a vesicular stomatitis virus (VSV) particle [the VSVΔG* system, in which the VSV G gene is replaced by the green fluorescent protein (GFP) gene] was reported previously to produce pseudotype VSV particles incorporating the envelope glycoproteins of several RNA viruses (i.e. measles virus, hantavirus, Ebola virus or hepatitis C virus; Matsuura *et al.*, 2001; Ogino *et al.*, 2003; Takada *et al.*, 1997; Tatsuo *et al.*, 2000). This system may be useful for research on viral envelope glycoproteins due to the ability of the pseudotype to grow at high titres in a variety of cell lines. The pseudotype virus titre obtained with the VSVΔG* system is generally higher than that of the pseudotype retrovirus system (Ogino *et al.*, 2003). Furthermore, infection of target cells with pseudotype VSV can be readily detected as GFP-positive cells by 16 h

Detection of expression of SARS-CoV-S protein and soluble mutated ACE2 are available as supplementary material in JGV Online.

post-infection (p.i.) because of the high level of GFP expression in the VSVΔG* system (Ogino *et al.*, 2003). In contrast, the time required for infection in the pseudotype retrovirus system is 48 h (Moore *et al.*, 2004; Nie *et al.*, 2004), which is similar to the time required for SARS-CoV to replicate to a level that results in plaque-forming or cytopathic effects in infected cells. To date, there have been no reports of VSV pseudotyped with the S protein of a coronavirus. Pseudotyping of SARS-CoV-S protein using the VSVΔG* system may have advantages for studying the functions of SARS-CoV-S protein, as well as for developing a rapid detection system to examine neutralizing antibodies specific for SARS-CoV infection.

To generate VSV pseudotyped with SARS-CoV-S protein, we first constructed an expression plasmid encoding full-length SARS-CoV-S protein. The cDNA of SARS-CoV-S protein was amplified using forward primer S-Bam-f (5′-GGATCCAAGTGATATTCTTGTTAACAAC-3′) and reverse primer S-Bam-r (5′-GGATCCAAGAGTAAAAAA-TCTCATAAAC-3′) and cloned into the expression vector pKS336 (Saijo *et al.*, 2002). The resulting plasmid, pKS-SARS-S, was transfected into 293T cells (see Supplementary Fig. S1, available in JGV Online), followed by infection with VSVΔG* (Matsuura *et al.*, 2001). When the culture supernatants of the infected 293T cells were inoculated on to Vero E6 cells, commonly used for SARS-CoV propagation, only small numbers of GFP-expressing cells were observed (data not shown). This result indicated that the VSV pseudotype bearing the full-length SARS-CoV-S protein was not very infectious. Next, we generated an expression plasmid encoding a C-terminal-truncated version of the SARS-CoV-S protein. The cDNA of C-terminal-truncated SARS-CoV-S protein was amplified from pKS-SARS-S using forward primer S-Bam-f and reverse primer S-Bam19r (5′-GGG-ATCCTTAGCAGCAAGAACCACAAGAGCATG-3′), followed by cloning into pKS336. The resulting plasmid, pKS-SARS-St19, encoded the full-length SARS-CoV-S protein except for the C-terminal 19 aa. When 293T cells were transfected with the expression plasmid pKS-SARS-St19, expression of the S protein was detected on the cell membrane (Supplementary Fig. S1). In contrast, transfection of the plasmid pKS-SARS-St19rev, in which the cDNA of C-terminal truncated SARS-CoV-S protein was inserted in the reverse orientation, did not show expression of SARS-CoV-S protein and was therefore used as a negative control for generating the VSV pseudotype. To generate a VSV pseudotype with the C-terminal truncated SARS-CoV-St19 protein, we inoculated VSVΔG* on to 293T cells transfected with either pKS-SARS-St19 or pKS-SARS-St19rev. VSVΔG*-G was used as a positive control, in which the deleted VSV-G protein was provided *in trans* encoded by pCAG-VSV-G (a kind gift from Dr Y. Matsuura, Osaka University, Japan) (Fig. 1a). The SARS-CoV-S protein-bearing VSV pseudotype, referred to as VSV-SARS-St19, obtained from 293T cells transfected with pKS-SARS-St19, efficiently infected Vero E6 cells (Fig. 1a). The titre of VSV-SARS-St19 was $5{\cdot}0 \times 10^5$ infectious units (IU) ml^{-1}. Since partial deletion of the SARS-CoV-S protein cytoplasmic domain allowed efficient incorporation into VSV particles and led to the generation of pseudotype at high titre, it was suggested that the intact cytoplasmic domain of SARS-CoV-S protein may have interrupted correct assembly of the pseudotype particles.

In order to confirm that the SARS-CoV-St19 protein was indeed incorporated into VSV particles, VSV pseudotypes were purified by ultracentrifugation using an RPS40T rotor (Hitachi) at 35 000 r.p.m. for 1 h through 20 % sucrose and then analysed by Western blotting using a rabbit antibody specific for aa 1124–1140 of SARS-CoV-S protein (Imgenex), a rabbit anti-VSV-G antibody (a kind gift from Dr S. Nagata, Tokyo University, Japan) and a mouse monoclonal antibody specific for VSV-M (a kind gift from Dr M. A. Whitt, GTx, Inc., TN, USA) (Fig. 1b). The VSV-M and SARS-CoV-S proteins were detected in VSV-SARS-St19, whereas the VSV-M and -G protein were detected in VSVΔG*-G. These results indicated that the SARS-CoV-St19 protein expressed in 293T cells was incorporated efficiently into VSV particles.

To determine the optimal incubation period for detection of VSV-SARS-St19 infection, we performed a time-course analysis of GFP expression. Vero E6 monolayers on 24-well glass slides were infected with VSV-SARS-St19. At various time points p.i., cells were photographed under a fluorescent microscope. The number of GFP-expressing cells in the photographs was counted using ImageJ software (http://rsb.info.nih.gov/ij/). Interestingly, GFP expression was detected clearly at 7 h p.i., although the fluorescence intensity of GFP expression was increased at 9 h p.i. (Fig. 1c). Infected cells detached from culture slides, presumably due to a cytopathic effect of VSV proteins, after incubation for 16 h (data not shown). As pseudoviruses are unable to produce progeny viruses, this system would be useful for the evaluation of cell entry mechanisms mediated by SARS-CoV-S protein. Therefore, the infection efficiency of VSV-SARS-St19 can be evaluated without incubation for up to 16 h p.i. Time-course analysis of the number of GFP-positive cells showed that quantification of VSV-SARS-St19 infection was possible at 7 h p.i. (Fig. 1c). Therefore, we counted the number of GFP-positive cells infected with VSV-SARS-St19 at 7 h p.i. for further study.

To confirm the specificity of infection, a rabbit anti-SARS-CoV antibody was tested for its ability to neutralize VSV-SARS-St19. The antibody was raised against UV-inactivated, purified SARS-CoV and reacted with SARS-CoV-S protein in an immunofluorescence assay (see Supplementary Fig. S1); the antibody showed neutralizing activity against SARS-CoV infection on Vero E6 cells at a dilution of 1 : 2560 (data not shown). As a negative control, we used a rabbit antibody raised against SARS-CoV-N protein-specific oligopeptides (Mizutani *et al.*, 2004). Culture medium containing 500 IU VSV-SARS-St19 was pre-incubated with serially diluted antibodies followed by inoculation on to Vero E6 cells. Pre-incubation with anti-SARS-CoV antibody showed

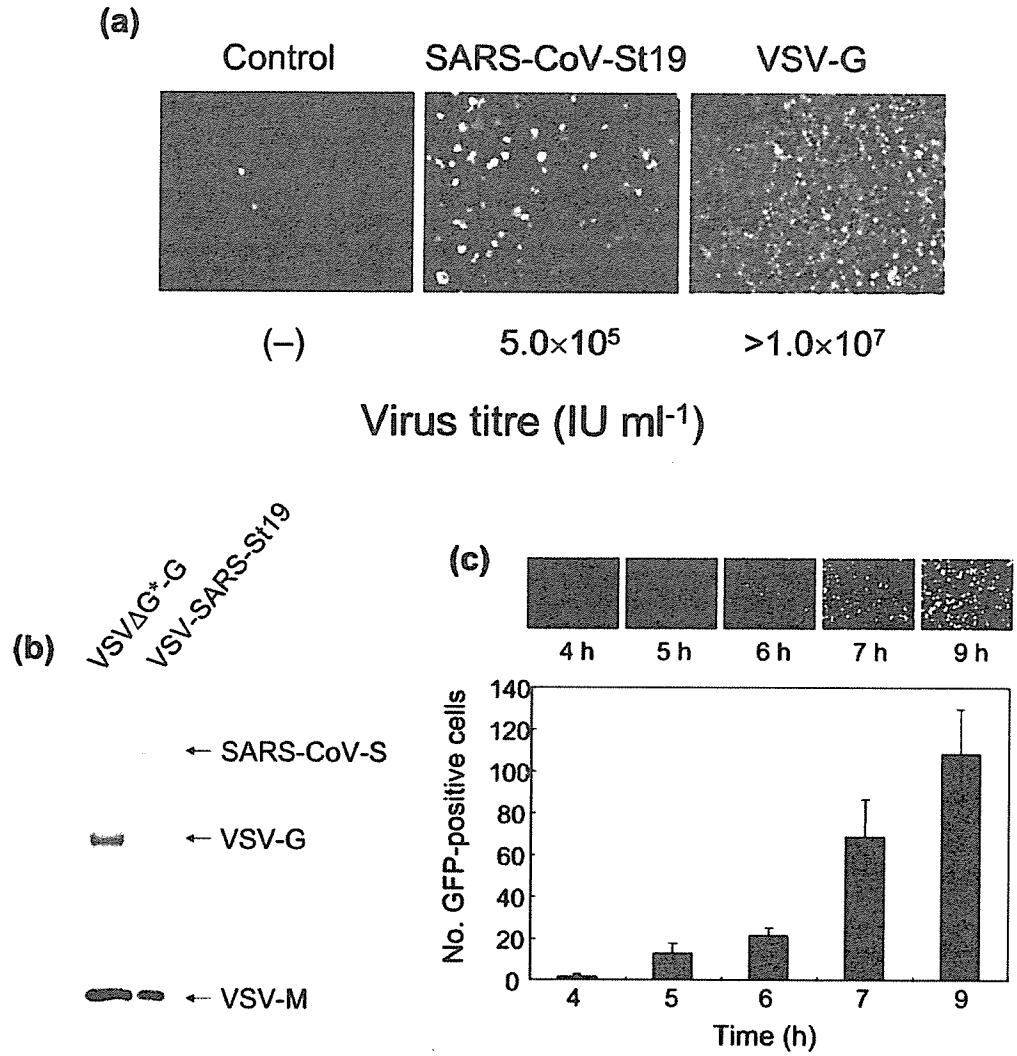

Fig. 1. Generation and characterization of VSV pseudotyped with SARS-CoV-S protein. (a) VSVΔG* was inoculated on to 293T cells expressing the indicated glycoproteins. After 24 h, culture supernatants were collected, filtered through a 0·22 μm pore size filter and inoculated on to Vero E6 cells. GFP expression was examined under a fluorescent microscope. The titre of pseudotypes viruses was determined by end-point dilution. (b) Incorporation of SARS-CoV-S protein into pseudotype VSV particles. VSV-SARS-St19 and VSVΔG*-G were partially purified by ultracentrifugation through 20 % sucrose. Viral proteins were analysed by Western blotting. The bands of SARS-CoV-S protein (180 kDa), VSV-G protein (62 kDa) and VSV-M protein (32 kDa) are indicated. (c) Rapid detection and quantification of VSV-SARS-St19 infection. Vero E6 cells were infected with VSV-SARS-St19 and GFP expression was examined at the indicated time points p.i. under a fluorescent microscope. The bar graph represents the number of GFP-positive cells per microscopic field (mean ± SD) calculated from six fields.

a significant reduction in the titre of VSV-SARS-St19 in a dose-dependent manner (Fig. 2a). Fifty per cent neutralizing activity was calculated at a dilution of 1 : 2000. In contrast, infection of Vero E6 cells with VSVΔG*-G was not affected by the anti-SARS-CoV antibody, even at a lower dilution (1 : 80 dilution) (Fig. 2a). When VSV-SARS-St19 was pre-incubated with control anti-SARS-CoV-N antibody, no neutralizing activity was observed (Fig. 2a). The possibility of carry-over of VSV-G during the production of VSV-SARS-St19, leading to infection of Vero E6 cells, was excluded, since an anti-VSV-G monoclonal antibody (P2F3, a kind gift from Dr. S. Nagata), which showed specific neutralizing activity against VSV infection (Nagata *et al.*, 1992), had no effect on infection of Vero E6 cells by VSV-SARS-St19 (Fig. 2b), but prohibited infection by VSVΔG*-G. These results indicated that infection of Vero E6 cells with

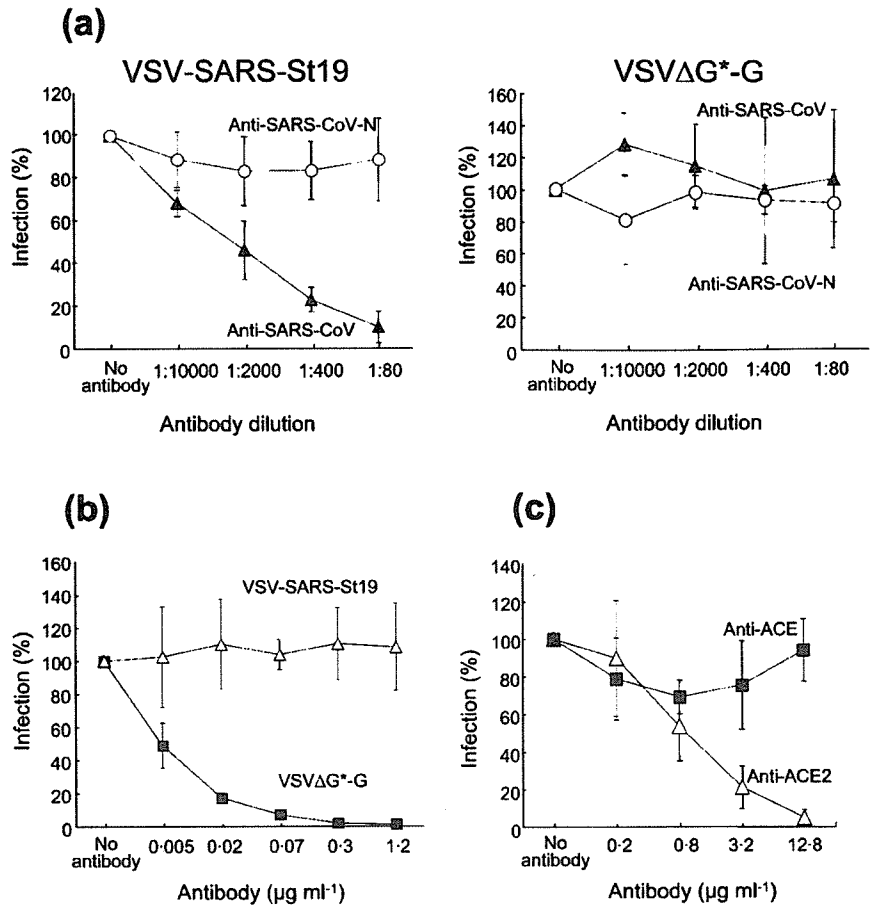

Fig. 2. Specificity of VSV-SARS-St19 pseudotype infection. (a) VSV-SARS-St19 (left) or VSVΔG*-G (right) was pre-incubated with serially diluted anti-SARS-CoV (▲) or anti-SARS-CoV-N (○) followed by inoculation on to Vero E6 cells. (b) VSV-SARS-St19 (△) or VSVΔG*-G (■) was pre-incubated with serially diluted anti-VSV-G antibody. (c) Vero E6 cells were pre-incubated with serially diluted anti-ACE (■) or anti-ACE2 (△) antibody and infected with VSV-SARS-St19. At 7 h p.i., GFP-positive cells were counted. The number of GFP-positive cells in the absence of antibodies was set as 100%. The results are shown as mean ± SD for at least three independent assays.

VSV-SARS-St19 was mediated solely by SARS-CoV-S protein.

To determine whether anti-ACE2 antibody could inhibit VSV-SARS-St19 infection, Vero E6 cells were pre-incubated with anti-ACE2 antibody (R&D Systems) and the infectivity of VSV-SARS-St19 was examined. As a negative control, cells were pre-incubated with anti-ACE antibody (R&D Systems). As shown in Fig. 2(c), pre-incubation with anti-ACE2 antibody resulted in a significant reduction in VSV-SARS-St19 infection in a dose-dependent manner. Anti-ACE2 antibody, at a concentration of 12·8 μg ml^{-1}, completely inhibited VSV-SARS-St19 infection. In contrast, anti-ACE antibody had no appreciable effect on infection. These results indicated that VSV-SARS-St19 infection is ACE2-dependent. These observations were consistent with those reported previously by Li *et al.* (2003); on SARS-CoV infection of Vero E6 cells, the same polyclonal antibody showed an inhibitory effect on cytopathicity in a dose-dependent manner and complete inhibition was observed at an anti-ACE2 antibody concentration of approximately 10 μg ml^{-1}.

We further analysed whether soluble ACE2 protein could inhibit infection by VSV-SARS-St19. We introduced two amino acid substitutions at aa 374 and 378 within the putative catalytic domain of ACE2 (soACE2-NN; Supplementary Fig. S2). Purified soACE2-NN protein expressed in a baculovirus expression system was pre-incubated with VSV-SARS-St19 or VSVΔG*-G and the mixtures inoculated on to Vero E6 cells. As shown in Fig. 3(a), soluble ACE2 protein strongly inhibited VSV-SARS-St19 infection in a dose-dependent manner, but did not affect VSVΔG*-G infection. These observations indicated that purified soluble ACE2 specifically inhibited VSV-SARS-St19 infection. The highest concentration of soACE2 showed partial inhibition

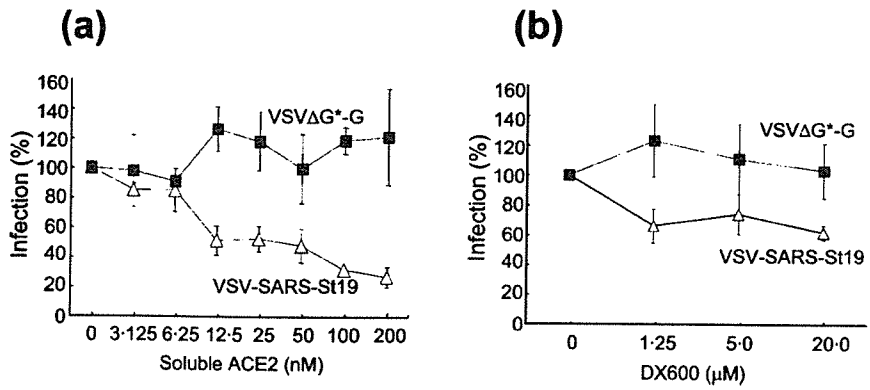

Fig. 3. Inhibition of VSV-SARS-St19 infection. VSV-SARS-St19 (△) or VSVΔG*-G (■) was pre-incubated with serially diluted soACE2NN (a) or DX600 (b), followed by inoculation on to Vero E6 cells. The infectivity of the pseudotypes was examined as described in Fig. 2.

(70–80 %) of VSV-SARS-St19 infectivity. However, the possibility that ACE2-independent entry of the pseudotype virus also existed could be excluded, since anti-ACE2 antibody completely inhibited VSV-SARS-St19 infectivity and almost all of the infection was dependent on ACE2 (Fig. 2c). The amount of soluble ACE2 that neutralized 50 % of the VSV-SARS-St19 infection (50 % neutralizing dose; ND_{50}) was estimated to be 12·5 nM. The neutralization activity of soACE2 in the present study was somewhat lower than that reported by Moore *et al.* (2004). This may have been due to the different strategies used for soACE2 preparation. The neutralization activity of soACE2 against SARS-CoV infection was lower than that of soluble mouse hepatitis virus receptor (soMHVR) against MHV infection (ND_{50} = 1 nM; Miura *et al.*, 2004; Zelus *et al.*, 1998). These observations suggested that SARS-CoV infection is regulated less strictly by the receptor function than MHV infection. Alternatively, a subdomain of ACE2 protein might represent increasing neutralization activity if bound to the SARS-CoV-S protein more strongly than the full-length protein. Indeed, neutralization of MHV-A59 infection was enhanced when the N-terminal subdomain of MHVR was used for neutralization experiments (Zelus *et al.*, 1998). It is noteworthy that an alternative splice variant of mouse ACE2 mRNA, consisting of the 5′ half of mouse ACE2 mRNA and not containing the metalloproteinase catalytic domain, has been reported (Komatsu *et al.*, 2002).

We then investigated whether a known ACE2-specific peptide inhibitor competed against ACE2-mediated pseudotype virus infection. VSV-SARS-St19 was pre-incubated with various concentrations of DX600 (Phoenix Pharmaceuticals), which has been shown to bind to and inhibit the enzymic activity of ACE2 (Huang *et al.*, 2003), and the mixture was then inoculated on to Vero E6 cells. Interestingly, DX600 inhibited VSV-SARS-St19 infection, but did not inhibit VSVΔG*-G infection. Higher concentrations (> 1·25 μM) of DX600 were required for 30–40 % inhibition, indicating that this inhibition was weak (Fig. 3b). It has been shown that enzymic activity is not required for ACE2 protein as a SARS-CoV receptor (Li *et al.*, 2003). However, our results indicated that incubation of DX600 partially influenced the ACE2 function as a SARS-CoV receptor. Further investigation including inhibition studies with live SARS-CoV will be needed to elucidate the efficacy of DX600. Our results suggest that ACE2-binding peptides can be used as specific inhibitors of SARS-CoV-S protein-mediated infection. Based on the results of neutralization experiments using anti-SARS-CoV antibody and anti-ACE2 antibody, we conclude that VSV-SARS-St19 infection of target cells is mediated by SARS-CoV-S protein. The assay system described here would be useful not only for developing a safe and rapid method of detecting neutralizing antibodies to SARS-CoV, but also for screening of inhibitors of SARS-CoV-S protein-mediated infection.

Acknowledgements

We thank Dr M. A. Whitt for providing the VSVΔG* and anti-VSV-M antibody, Dr S. Nagata for providing monoclonal antibody P2F3 and rabbit anti-VSV G antibody, and Dr Y. Matsuura for providing pCAG-VSVG. We also thank Ms M. Ogata for her assistance. This work was supported in part by a grant-in-aid from the Ministry of Health, Labor and Welfare of Japan and the Japan Health Science Foundation, Tokyo, Japan.

References

Drosten, C., Gunther, S., Preiser, W. & 23 other authors (2003). Identification of a novel coronavirus in patients with severe acute respiratory syndrome. *N Engl J Med* 348, 1967–1976.

Fouchier, R. A., Kuiken, T., Schutten, M. & 7 other authors (2003). Aetiology: Koch's postulates fulfilled for SARS virus. *Nature* 423, 240.

Giroglou, T., Cinatl, J., Jr, Rabenau, H., Drosten, C., Schwalbe, H., Doerr, H. W. & von Laer, D. (2004). Retroviral vectors pseudotyped with severe acute respiratory syndrome coronavirus S protein. *J Virol* 78, 9007–9015.

Hofmann, H., Geier, M., Marzi, A., Krumbiegel, M., Peipp, M., Fey, G. H., Gramberg, T. & Pohlmann, S. (2004). Susceptibility to SARS coronavirus S protein-driven infection correlates with expression of angiotensin converting enzyme 2 and infection can be blocked by soluble receptor. *Biochem Biophys Res Commun* **319**, 1216–1221.

Huang, L., Sexton, D. J., Skogerson, K. & 13 other authors (2003). Novel peptide inhibitors of angiotensin-converting enzyme 2. *J Biol Chem* **278**, 15532–15540.

Komatsu, T., Suzuki, Y., Imai, J., Sugano, S., Hida, M., Tanigami, A., Muroi, S., Yamada, Y. & Hanaoka, K. (2002). Molecular cloning, mRNA expression and chromosomal localization of mouse angiotensin-converting enzyme-related carboxypeptidase (mACE2). *DNA Seq* **13**, 217–220.

Ksiazek, T. G., Erdman, D., Goldsmith, C. S. & 23 other authors (2003). A novel coronavirus associated with severe acute respiratory syndrome. *N Engl J Med* **348**, 1953–1966.

Li, W., Moore, M. J., Vasilieva, N. & 9 other authors (2003). Angiotensin-converting enzyme 2 is a functional receptor for the SARS coronavirus. *Nature* **426**, 450–454.

Marra, M. A., Jones, S. J., Astell, C. R. & 56 other authors (2003). The genome sequence of the SARS-associated coronavirus. *Science* **300**, 1399–1404.

Matsuura, Y., Tani, H., Suzuki, K. & 8 other authors (2001). Characterization of pseudotype VSV possessing HCV envelope proteins. *Virology* **286**, 263–275.

Miura, H. S., Nakagaki, K. & Taguchi, F. (2004). N-terminal domain of the murine coronavirus receptor CEACAM1 is responsible for fusogenic activation and conformational changes of the spike protein. *J Virol* **78**, 216–223.

Mizutani, T., Fukushi, S., Saijo, M., Kurane, I. & Morikawa, S. (2004). Phosphorylation of p38 MAPK and its downstream targets in SARS coronavirus-infected cells. *Biochem Biophys Res Commun* **319**, 1228–1234.

Moore, M. J., Dorfman, T., Li, W. & 9 other authors (2004). Retroviruses pseudotyped with the severe acute respiratory syndrome coronavirus spike protein efficiently infect cells expressing angiotensin-converting enzyme 2. *J Virol* **78**, 10628–10635.

Nagata, S., Okamoto, Y., Inoue, T., Ueno, Y., Kurata, T. & Chiba, J. (1992). Identification of epitopes associated with different biological activities on the glycoprotein of vesicular stomatitis virus by use of monoclonal antibodies. *Arch Virol* **127**, 153–168.

Nie, Y., Wang, P., Shi, X. & 13 other authors (2004). Highly infectious SARS-CoV pseudotyped virus reveals the cell tropism and its correlation with receptor expression. *Biochem Biophys Res Commun* **321**, 994–1000.

Ogino, M., Ebihara, H., Lee, B. H., Araki, K., Lundkvist, A., Kawaoka, Y., Yoshimatsu, K. & Arikawa, J. (2003). Use of vesicular stomatitis virus pseudotypes bearing Hantaan or Seoul virus envelope proteins in a rapid and safe neutralization test. *Clin Diagn Lab Immunol* **10**, 154–160.

Rota, P. A., Oberste, M. S., Monroe, S. S. & 32 other authors (2003). Characterization of a novel coronavirus associated with severe acute respiratory syndrome. *Science* **300**, 1394–1399.

Saijo, M., Qing, T., Niikura, M., Maeda, A., Ikegami, T., Sakai, K., Prehaud, C., Kurane, I. & Morikawa, S. (2002). Immunofluorescence technique using HeLa cells expressing recombinant nucleoprotein for detection of immunoglobulin G antibodies to Crimean-Congo hemorrhagic fever virus. *J Clin Microbiol* **40**, 372–375.

Simmons, G., Reeves, J. D., Rennekamp, A. J., Amberg, S. M., Piefer, A. J. & Bates, P. (2004). Characterization of severe acute respiratory syndrome-associated coronavirus (SARS-CoV) spike glycoprotein-mediated viral entry. *Proc Natl Acad Sci U S A* **101**, 4240–4245.

Takada, A., Robison, C., Goto, H., Sanchez, A., Murti, K. G., Whitt, M. A. & Kawaoka, Y. (1997). A system for functional analysis of Ebola virus glycoprotein. *Proc Natl Acad Sci U S A* **94**, 14764–14769.

Tatsuo, H., Okuma, K., Tanaka, K., Ono, N., Minagawa, H., Takade, A., Matsuura, Y. & Yanagi, Y. (2000). Virus entry is a major determinant of cell tropism of Edmonston and wild-type strains of measles virus as revealed by vesicular stomatitis virus pseudotypes bearing their envelope proteins. *J Virol* **74**, 4139–4145.

Zelus, B. D., Wessner, D. R., Williams, R. K., Pensiero, M. N., Phibbs, F. T., deSouza, M., Dveksler, G. S. & Holmes, K. V. (1998). Purified, soluble recombinant mouse hepatitis virus receptor, $Bgp1^b$, and Bgp2 murine coronavirus receptors differ in mouse hepatitis virus binding and neutralizing activities. *J Virol* **72**, 7237–7244.

Jpn. J. Infect. Dis., 58, 88-94, 2005

Original Article

Immunological Detection of Severe Acute Respiratory Syndrome Coronavirus by Monoclonal Antibodies

Kazuo Ohnishi, Masahiro Sakaguchi, Tomohiro Kaji, Kiyoko Akagawa, Tadayoshi Taniyama, Masataka Kasai, Yasuko Tsunetsugu-Yokota, Masamichi Oshima, Kiichi Yamamoto, Naomi Takasuka, Shu-ichi Hashimoto, Manabu Ato, Hideki Fujii, Yoshimasa Takahashi, Shigeru Morikawa[1], Koji Ishii[2], Tetsutaro Sata[4], Hirotaka Takagi[5], Shigeyuki Itamura[3], Takato Odagiri[3], Tatsuo Miyamura[2], Ichiro Kurane[1], Masato Tashiro[3], Takeshi Kurata[6], Hiroshi Yoshikura[6] and Toshitada Takemori*

Department of Immunology, [1]Department of Virology I, [2]Department of Virology II, [3]Department of Virology III, [4]Department of Pathology and [5]Division of Biosafety Control and Research, [6]National Institute of Infectious Diseases, Tokyo 162-8640, Japan

(Received October 20, 2004. Accepted February 14, 2005)

SUMMARY: In order to establish immunological detection methods for severe acute respiratory syndrome coronavirus (SARS-CoV), we established monoclonal antibodies directed against structural components of the virus. B cell hybridomas were generated from mice that were hyper-immunized with inactivated SARS-CoV virion. By screening 2,880 generated hybridomas, we established three hybridoma clones that secreted antibodies specific for nucleocapsid protein (N) and 27 clones that secreted antibodies specific for spike protein (S). Among these, four S-protein specific antibodies had in vitro neutralization activity against SARS-CoV infection. These monoclonal antibodies enabled the immunological detection of SARS-CoV by immunofluorescence staining, Western blot or immunohistology. Furthermore, a combination of monoclonal antibodies with different specificities allowed the establishment of a highly sensitive antigen-capture sandwich ELISA system. These monoclonal antibodies would be a useful tool for rapid and specific diagnosis of SARS and also for possible antibody-based treatment of the disease.

INTRODUCTION

The outbreak of severe acute respiratory syndrome (SARS) in 2003, caused by SARS coronavirus (SARS-CoV)(1,2), ultimately led to 8,000 people becoming infected, 916 of whom died (3; http://who.int/csr/sars/country/en/country2003_08_15.pdf). Even though the WHO announced an end to the epidemic (4; http://www.who.int/entity/csr/sars/resources/en/SARSReferenceLab1.pdf), the threat of re-emergence persists due to the absence of a vaccine, and inability of health services to rapidly detect and specifically diagnose the disease. One of the critical issues in the management of clinical patients and control of the pandemic is a system of early diagnosis that distinguishes SARS from other types of pulmonary infections. As an epidemiological history of contact with SARS patients is not always provable and there are no clinical signs unique to SARS patients (5), confirmatory diagnosis relies primarily on laboratory tests.

To date, viral shedding of SARS-CoV has been extensively studied to improve diagnosis and infectious control (6-8). Maximum virus shedding takes place between day 12 and day 14 of disease onset. For most acute respiratory viral infections, viral shedding occurs within the first few days from the nasopharyngeal tissue and soon after at the upper respiratory tract, but seldom lasts for more than 10 days (6-8). The peak of shedding in stools occurs a few days after respiratory shedding and remains high even after 3 weeks (7, 8). SARS-CoV was detected in patients' plasma samples within several days of the onset of fever, sometimes at levels equivalent to those recorded for nasopharyngeal aspirates (6, 9).

Previously, during the outbreak in Hong Kong (8), laboratory diagnosis for SARS virus infection was based on a combination of serologic tests, reverse transcription-polymerase chain reaction (RT-PCR), and virus isolation. IgG seroconversion among those infected was 93% by day 28 (5), suggesting that while antibody seroconversion provides reliable proof of infection (5,10); it is, however, not suitable for early diagnosis (11). Among patients in whom the serological evidence could be retrospectively examined, RT-PCR provided about 60% of the diagnostic yield using tracheal aspirates and stools for the first 2 weeks after the onset of illness (8). Although the availability of data that compares the diagnostic yield of various specimen types is still limited, it has been suggested that a combination of stool samples and pooled throat and nasal swab specimens provides reagents for safe and high-yield SARS-CoV detection (8). Furthermore, in addition to RT-PCR on respiratory and fecal samples, serology is needed to confirm the diagnosis of SARS-CoV infection in most cases.

Based on clinical experience, several options have been considered in the quest to develop the capacity to accurately diagnose SARS-CoV infection, including molecular biology techniques and serological tests such as antigen-captured ELISA assay and immunofluorescence assay to detect virus-infected cells in respiratory swabs (5-12). The preparation of monoclonal antibodies (mAbs) is considered to be valuable especially for serological testing.

*Corresponding author: Mailing address: Department of Immunology, National Institute of Infectious Diseases, Toyama 1-23-1, Shinjuku-ku, Tokyo 162-8640, Japan. Tel: +81-3-5285-1111, Fax: +81-5285-1150, E-mail: ttoshi@nih.go.jp

In this paper we report the successful establishment and the characterization of mAbs against SARS-CoV structural components. These mAbs enabled the general immunological detection of SARS-CoV, by the methods such as immunofluorescent staining, Western blotting, and immunohistology, in addition to the construction of highly sensitive antigen-capture sandwich ELISA.

MATERIALS AND METHODS

Virus and cell culture: SARS-CoV (HKU-39849) was kindly supplied by Dr. J. S. M. Peiris, Department of Microbiology, the University of Hong Kong. The live virus was manipulated under the physical containment level P3. For the purification of the virion, the day-2 culture supernatant of Vero E6, which had been infected with SARS-CoV at moi = 1.0, was centrifuged at 8,000×g for 30 min to remove cell debris. The virion in the supernatant was precipitated with 8% polyethylene glycol/ 0.5 M NaCl, and further purified by 20%/60%-discontinuous sucrose density gradient centrifugation. This fraction was inactivated by UV-irradiation (260 nm, 4.75 J/cm^2), and used as UV-inactivated SARS-CoV fraction. We and others confirmed that this condition completely inactivates SARS-CoV (13,14).

Production of mAbs: BALB/c mice (9-week old females, Japan SLC) were immunized subcutaneously with 20 μg of UV-inactivated SARS-CoV using Freund's Complete Adjuvant (FCA, Sigma, St. Louis, Mo., USA). After 2 weeks, the mice were boosted with a subcutaneous injection of 5 μg of UV-inactivated SARS-CoV using Freund's Incomplete Adjuvant (FIA, Sigma). On day-3 after the boost, sera from the mice were tested by ELISA for the antibody titer against SARS-CoV. The two mice showing highest antibody titer were further boosted intravenously with 5 μg of the inactivated virus 14 days after the previous boost. This immunization schedule was called protocol-1. In protocol-2 the booster injection was repeated two more times before the final boost. Three days after the final boost, spleens from two mice were excised and the splenocytes were fused with Sp2/O-Ag14 myeloma by the polyethylene glycol method of Kozbor and Roder (15). The fused cells from the two spleens were cultured and HAT-selected on twenty 96-well plates. The first screening was conducted by ELISA using SARS-CoV infected Vero E6 cell lysate as the antigen. In this first screening, the ELISA with uninfected Vero E6 cell lysate was used as the negative control. After the virus was inactivated by UV-irradiation, cell lysates were prepared by NP-40 lysis buffer (1% NP-40/ 150 mM NaCl/ 50 mM Tris, pH 7.5) followed by centrifugation at 15,000 rpm for 20 min to remove the cell debris. The supernatant was diluted 100-fold using ELISA-coating buffer (50 mM sodium bicarbonate, pH 9.6) and the ELISA plates (Dynatech, Chantily, Va., USA) were coated at 4°C overnight. After blocking with 1% ovalbumin in PBS-Tween (10 mM phosphate buffer, 140 mM NaCl, 0.05% Tween 20, pH 7.5) for 1 h, the culture supernatants from HAT-selected hybridomas were added and incubated for 1 h. After washing with PBS-Tween, the bound antibodies were detected with alkaline phosphatase-conjugated anti-mouse IgG (1:2000, Zymed, South San Francisco, Calif., USA) using *p*-nitrophenyl phosphate (PNPP) as a substrate. The second screening was conducted by ELISA using the cell lysates of chick embryonic fibroblast (CEF) cell lines that were transfected by vaccinia virus vector containing the gene either of SARS-CoV spike (S) or nucleocapsid (N) proteins.

Recombinant virus proteins: Genomic RNA was extracted from SARS-CoV strain HKU39849 and reverse transcribed to cDNA. The corresponding open reading frames (ORF) to E, M, N and S were amplified by PCR and cloned into the transfer vector, pDIsgptmH5, which also harbored *Escherichia coli* xantine-guanine phosphoribosyltransferase under the control of vaccinia virus p7.5 promoter in the cloning site of pUc/DIs (16). The recombinant clones of attenuated vaccinia virus, DIs, which harbored each ORF were obtained by homologous recombination induced in DIs-infected-, pDIsgptmH5-transfected CEF cells. The detailed protocol will be published elsewhere.

Neutralization assay: The known tissue culture infectious dose (TCID) of SARS-CoV was incubated for 1 h in the presence or absence of the purified mAbs serially diluted 10-fold, and then added to Vero E6 cell culture grown to confluence in a 96-well microtiter plate. As a control, mAbs against N protein was added to the culture. After 48 hr, cells were fixed with 10% formaldehyde and stained with crystal violet to visualize the cytopathic effect induced by the virus (17). Neutralization antibody titers were expressed as the minimum concentration of purified immunoglobulin that inhibits cytopathic effect.

Western blot: UV-inactivated purified SARS-CoV virion (0.5 μg/lane)(13) was loaded on SDS-PAGE under reduced conditions. Proteins were transferred to the PVDF membrane (Genetics, Tokyo, Japan). After blocking with BlockAce (Snow Brand Milk Products Co., Ltd., Tokyo, Japan) reagent, the membranes were reacted with the mAbs or the diluted sera (1:1000) that had been obtained from mice inoculated with UV-irradiated SARS-CoV. After washing, the membrane was reacted with peroxidase-conjugated F(ab')$_2$ fragment anti-mouse IgG (H+L) (1:20,000 Jackson Immuno Research, West Grove, Pa., USA), and the bands were visualized using chemiluminescent reagents (Amasham Biosciences, Piscataway, N.J., USA) on the X-ray film (Kodak, Rochester, N.Y., USA).

Purification and biotinylation of mAbs: Hybridomas were grown in Hybridoma-SFM medium (Invitrogen, Carlsbad, Calif., USA) supplemented with recombinant IL-6 (18) and penicillin (100 U/mL)/streptomycin (100 μg/mL). The culture supernatants were harvested, added with 1/100 volume of 1 M Tris-HCl (pH 7.4) and 1/500 volume of 10% NaN_3, and directly loaded on the Protein G-Sepharose 6B column (Amersham Biosciences). The column was washed with PBS and eluted with Glycine/HCl (pH 2.8). After measuring the OD_{280} of the fractions, protein containing fractions were pooled and added with an equal volume of saturated $(NH_4)_2SO_4$. Precipitated proteins were dissolved in PBS, dialysed against PBS and stored at −20°C. The purified antibodies were biotinylated using sulfo-NHS-LC-biotin (Pierce, Rockford, Ill., USA) according to the manufacturer's protocol.

Antigen-capture ELISA: The purified mAb for the antigen-capture was immobilized on the microplate (Immulon 2, Dynatech) by incubating 4 μg/mL antibody in 50 mM sodium bicarbonate buffer (pH 8.6) at 4°C overnight. The microplate was blocked with 1% BSA, washed with PBS-Tween, and reacted with serial dilution of UV-inactivated purified SARS-CoV for 1 h at room temperature. After washing with PBS-Tween, wells were reacted with biotinylated probing mAb (0.1 μg/mL) for 1 h at room temperature. After washing, wells were reacted with β-D-galactosidase-labeled streptavidine (Zymed) for 1 h at room temperature. After washing,

fluorescent substrate 4-methylumberyferyl-β-D-galactoside (Sigma-Aldrich, St. Louis, Mo., USA) was added and the substrate was incubated for 2 h at 37°C. The reaction was stopped by adding 0.1M Glycine-NaOH (pH 10.2) and the fluorescence (FU) of the reaction product, 4-methylumberiferron, was measured using FluoroScan (Flow Laboratories Inc., Inglewood, Calif., USA).

Histology: Formaldehyde-fixed human lung tissue that was RT-PCR positive for SARS-CoV (19) and lung from a SARS-CoV infected macaque were embedded in paraffin and sectioned using the standard method. After de-paraffinization by standard method, the sections were soaked with 0.1 M citrate-buffer (pH 6.0) and autoclaved for 10 min at 121°C to inactivate viruses. Endogenous peroxidase was inactivated by 0.3% hydrogen peroxide for 30 min at room temperature. After blocking with 5% normal goat serum for 10 min, sections were incubated with the mAb at 4°C overnight. The bound antibody was detected by biotinylated anti-mouse IgG followed by peroxidase-labeled streptavidin (LSAB2 kit, DakoCytomation, Kyoto, Japan) and visualized with 0.2 mg/mL 3,3′-diaminobenzidine in 0.015% hydrogen peroxide/0.05M Tris-HCl (pH 7.6). The sections were counterstained with hematoxylin.

RESULTS

In order to establish the hybridomas that secrete specific mAbs to SARS-CoV, we immunized BALB/c mice with purified SARS-CoV whole virion fraction. The virus was inactivated by UV-irradiation to avoid a change in antigenicity presumably caused by aldehyde-fixation or detergent-solubilization. The immunization protocols used were those of the standard method in which the boost administrations were repeated twice (protocol-1) or four times (protocol-2) with 2-week intervals using FCA/FIA as an adjuvant (see Materials and Methods). Three days after the final boost, a single cell suspension was prepared from two spleens of immunized mice and fused with SP-2/O myeloma by a polyethylene-glycol method, the fused cells were then HAT-selected (15).

In the experiment with immunization protocol-1, we found that the culture supernatants from 28 of the 1,920 wells were strong-positive in ELISA testing in which the cell-lysate of SARS-CoV infected Vero E6 cells was used as a coated antigen (Table 1). As a negative control, we used uninfected Vero E6 cell-lysate as the antigen. Wells that showed a positive reaction were omitted from the count. Among the 28 wells, 19 reacted to vaccinia vector-based recombinant-S-protein and three reacted to recombinant-N-protein. These hybridomas were successfully cloned by a repeated limiting dilution method. The remaining six wells did not give rise to a significant positive signal to recombinant-S, -N or -M proteins. One anti-S mAb cross-reacted to porcine transmissible gastroenteritis virus (TGEV) and this clone was also omitted from further studies. None of these mAbs cross-reacted to mouse hepatitis virus (MHV).

The avidities of these cloned mAbs were tested by avidity-ELISA in the presence of urea. Although in the presence of 6 M urea some anti-S mAbs retained 18-35% of the original reactivity, less than 10% of the original reactivity remained in the presence of 8 M urea (Table 2). Three anti-N mAbs showed a very low avidity index in this assay system.

In a previous report that studied human IgG avidity maturation after rubella vaccination, high-avidity antibodies were defined as those that retain more than 50% of reactivity in the presence of 8 M urea (20). Although it would not be possible to directly apply this definition of polyclonal antibodies to our mAb case, the avidities of mAbs we obtained did not seem particularly high. This prompted us to attempt to obtain better mAbs with higher avidity by repeating booster immunization in anticipation of affinity maturation. After an additional two boosts, hybridomas were established by the same procedure as the first experiment. We screened 960 wells and obtained 14 wells positive for ELISA with SARS-CoV infected Vero E6 cell lysate (Table 1). Among the 14 wells, seven reacted with recombinant-S protein and none of them reacted with recombinant-N or -M proteins. These anti-S antibodies showed significantly higher avidity in the avidity ELISA (two representative clones are shown in Table 2). From the results of this avidity test, we selected five anti-S mAbs that showed the highest avidity index. None of these mAbs cross-reacted to human coronavirus, 229E (data not shown). These five anti-S and three anti-N mAbs were purified, and characterized further.

Table 1. Summary of the first hybridoma screening by ELISA

Immobilized antigen	Experiment-1[1)]	Experiment-2[2)]	Total
(Total wells assayed)	1,920	960	2,880
SARS-CoV infected Vero cell-lysate	28	14	42
Recombinant - S	19	7	26
- N	3	0	3

[1)]: Immunization protocol-1
[2)]: Immunization protocol-2

Table 2. Avidity ELISA

Clone	Epitope	Avidity Index (%)		
		4M urea	6M urea	8M urea
Experiment-1				
SKOT-7	N	1.6	1.2	1.5
SKOT-8	N	2.3	3.2	3.7
SKOT-9	N			
SKOT-3	S	45.5	18.7	1.2
SKOT-10	S	73.4	29.9	2.6
SKOT-20	S	63.8	35.4	8.8
Experiment-2				
SOAT-5	S	51.3	48.0	43.3
SOAT-13	S	77.0	62.0	48.0

All selected mAbs worked successfully in the immunofluorescent staining assay (Fig. 1). Anti-S mAbs such as SKOT-3, -10, -20, SOAT-5 and -13 stained the Golgi body and surface membrane of virus-infected cells but not of uninfected-cells. In contrast, the staining patterns of anti-N mAbs such as SKOT-7, -8 and -9 were mainly confined to the Golgi body.

All anti-N mAbs worked in immunohistochemistry of formalin-fixed, paraffin-embedded sections of both human lung from SARS patients and SARS-CoV infected macaque lung (Fig. 2). The specificity of these stainings was confirmed by the negative results for normal lungs and several specimens from pneumonia patients including cases complicated by measles, influenza type A, herpes-simplex and herpes zoster.

The mAbs that worked for immunohistochemistry, i.e.,

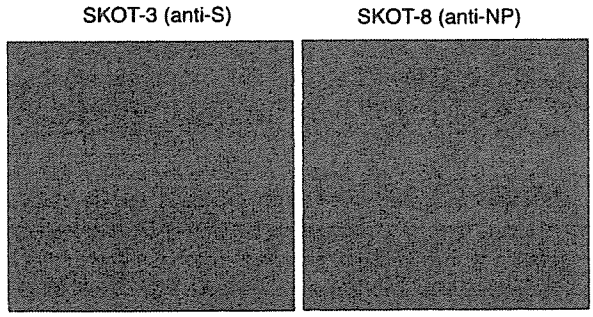

Fig. 1. Fluorescent immunostaining of SARS-CoV infected Vero E6 cells with monoclonal antibodies (mAbs). Parformaldehyde-fixed, SARS-CoV infected Vero E6 cells were permeabilized with TBS-tween and incubated with mAbs from hybridoma clones and the antibodies were detected with FITC-conjugated anti-mouse IgG. Shown are representative staining patterns with anti-S mAb, SKOT-3 (A), and anti-N mAb, SKOT-8 (B).

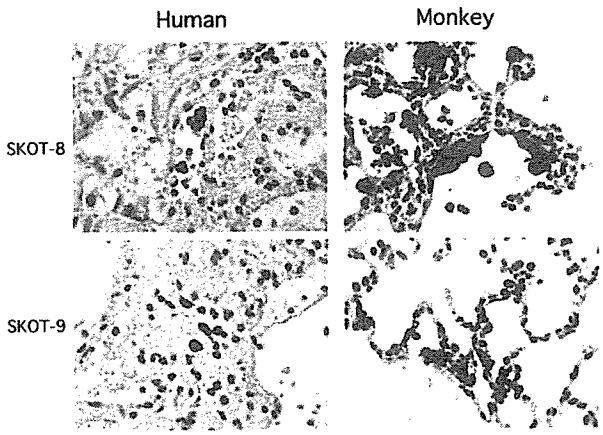

Fig. 2. Immuno-histochemistry of SARS-CoV infected human lung and macaque lung tissues with mAbs. Paraformaldehyde-fixed, paraffin-embedded sections were incubated with mAbs, and then with biotinylated anti-mouse IgG/peroxidase-labeled streptavidin complex before being visualized using DAB as a peroxidase substrate. Counter-staining with hematoxilin. Shown are human patient lung tissue (left panels) and SARS-infected macaque lung tissues (right panels), stained with anti-N mAbs (SKOT-8, SKOT-9).

SKOT-7, -8 and -9 also worked for Western-blot detection of the viral proteins (Fig. 3). Anti-N mAbs detected a band of 50 kDa that corresponds to the calculated molecular weight of SARS-CoV N-protein. In some experiments with longer exposure, a band with an apparent molecular weight of 120 kDa was also detected. None of the anti-S mAbs worked in the Western blot, suggesting that the major antigenic determinants of the S-protein are 'conformational' epitopes.

We tested the in vitro neutralizing activities of anti-S mAbs. As shown in Fig. 4, SKOT-20 neutralized in vitro SARS-CoV infection to Vero E6 cells at an antibody concentration of 1 μg/mL. Another anti-S mAb, SKOT-19, which had a low avidity value, also showed similar neutralizing activity. SKOT-10 and -3 also had neutralization activity but required higher antibody concentrations.

Lastly, we tried to construct an antigen-capture detection system for SARS-CoV by sandwich ELISA. In preliminary experiments, we tested all the combinations of two mAbs from the selected eight mAbs to obtain the highest detection sensitivity for purified SARS-CoV virion, and found that the

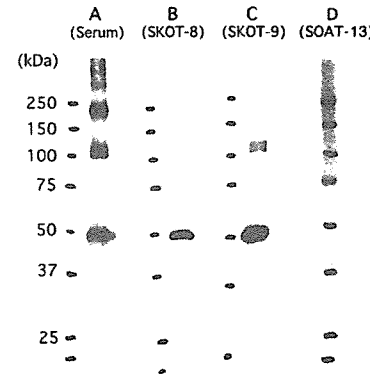

Fig. 3. Detection of virus proteins with Western blot. Purified SARS-CoV proteins (0.5 μg/lane) were electrophoresed with SDS-PAGE under reducing conditions. After blotting on the PVDF membrane, proteins were detected by incubation with mAbs, followed by incubation with peroxidase labeled-F(ab')$_2$ fragment of Donkey anti-mouse IgG. They were then visualized by chemiluminescent reaction. A: mouse serum from SARS-CoV immunized mouse; B: anti-N mAb, SKOT-8; C: anti-N mAb, SKOT-9; D: anti-S mAb, SOAT-13. The positions of molecular weight markers are shown on the left.

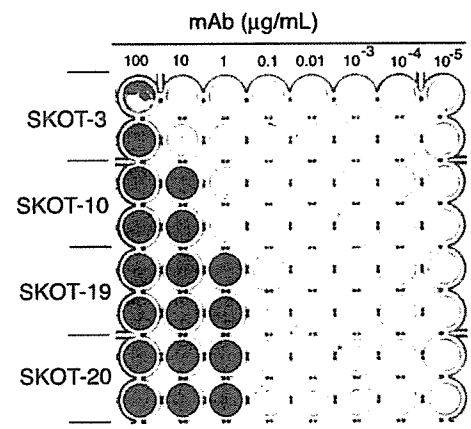

Fig. 4. In vitro neutralization assay of SARS-CoV infection with mAbs. Purified SARS-CoV fraction was diluted to 1×10^2 PFU/mL and incubated with serially-titrated purified mAbs for 1 h at 37°C. After the reaction, samples were poured into wells of a 96-well plate on which Vero E6 cells were grown to 90% confluent. After 48 h, cytotoxicities were visualized by staining the cells with crystalviolet. The results of purified anti-S antibodies (SKOT-3, -10, -19 and -20) with concentrations ranging from 100 μg/mL to 10^{-5} μg/mL are shown.

immobilization of SKOT-8 on the ELISA plate followed by the detection with biotinylated SKOT-9 gave the best result (data not shown; see Materials and Methods). In this sandwich ELISA, SARS-CoV protein was successfully detected in a concentration as low as 40 pg/mL (Fig. 5). Since the mAbs were originally raised against SARS-CoV strain HKU39849, we tested the validity of this system for other strains of SARS-CoV. As shown in Fig. 6, it was confirmed that the strains HK14T1WL, CDC00592 and Frankfurt1 were as detectable as HKU39849 using this system.

DISCUSSION

We established mAbs against SARS-CoV, which enable